DNA origami-based *in vitro* delivery vehicles

Erika Järvihaavisto

School of Electrical Engineering

Thesis submitted for examination for the degree of Master of Science in Technology.

Espoo 25.3.2016

Thesis supervisor:

Prof. Mauri Kostiainen

Thesis advisor:

Ph.D., Docent Veikko Linko

Aalto University
School of Electrical
Engineering

AALTO UNIVERSITY
SCHOOL OF ELECTRICAL ENGINEERING

ABSTRACT OF THE
MASTER'S THESIS

Author: Erika Järvihaavisto

Title: DNA origami-based *in vitro* delivery vehicles

Date: 25.3.2016 Language: English Number of pages: 8+60

Department of Biotechnology and Chemical Technology

Professorship: Polymer technology

Supervisor: Prof. Mauri Kostiainen

Advisor: Ph.D., Docent Veikko Linko

The field of DNA nanotechnology aims to construct artificial nanoscale structures and functionalized materials from DNA. The rapid development of DNA nanotechnology has inspired researchers to develop various DNA-based drug delivery vehicles. One approach to build complex DNA nanostructures is to use the method of DNA origami, which is discussed in more detail in this thesis.

This thesis examines the use of a tubular DNA origami as a cellular delivery vehicle for the transport of Streptavidin-Lucia luciferase enzymes into HEK293 cells *in vitro*. The correct folding of the origamis was evaluated using agarose gel electrophoresis and transmission electron microscopy. The transfection was studied using confocal microscopy and the activity of the delivered enzymes was detected in the cell lysates using a bioluminescence assay. These DNA origami-enzyme complexes were also coated with varying amounts of different cationic block-copolymers, and the effect of these coatings on the enzyme activity was investigated using the bioluminescence assay.

According to the results, the DNA origami delivered the enzymes into cells and the enzymes remained active after transfection. The results also suggest that it is possible to control the enzyme kinetics of the complexes by varying the amount of cationic polymers that coat the DNA origamis. However, the enzymes were found to bind nonspecifically to the origamis, and it remains unclear whether the shape of the origami contributed to the transfection. The stability and integrity of the complexes should be studied more carefully.

Keywords: DNA origami, DNA nanotechnology, drug delivery vehicle, Streptavidin-Lucia luciferase enzyme, *in vitro*

AALTO-YLIOPISTO
SÄHKÖTEKNIIKAN KORKEAKOULU

DIPLOMITYÖN
TIIVISTELMÄ

Tekijä: Erika Järvihaavisto

Työn nimi: DNA-origami-pohjaiset *in vitro* -kuljettimet

Päivämäärä: 25.3.2016 Kieli: Englanti Sivumäärä: 8+60

Biotekniikan ja kemian tekniikan laitos

Professuuri: Polymeeriteknologia

Työn valvoja: Prof. Mauri Kostiainen

Työn ohjaaja: FT, dosentti Veikko Linko

DNA-nanoteknologia tarkoittaa keinotekoisten nanomittakaavan rakenteiden ja funktionaalisten materiaalien muodostamista DNA:sta. DNA-nanorakenteiden nopea kehitys on innostanut tutkijoita kehittämään niistä erilaisia lääkeainekuljettimia kohdennettuun lääkeannosteluun. Monimutkaisia DNA-rakenteita voidaan muodostaa muun muuassa DNA-origami-tekniikalla, jota käsitellään tässä diplomityössä tarkemmin.

Tässä diplomityössä tutkitaan putkimaisen DNA-origamin soveltuvuutta kuljettaa Streptavidin-Lucia luciferase -entsyymejä HEK293-solujen sisään *in vitro*. Transfektiota tutkittiin konfokaalimikroskoopilla, ja entsyymien aktiivisuutta solujen lysaateissa tarkasteltiin mittaamalla bioluminesenssia. Nämä DNA-origami-entsyymikompleksit päällystettiin myös kolmella erilaisella kationisella blokkipolymeerilla. Polymeeripeitteiden vaikutusta entsyymin aktiivisuuteen tutkittiin mittaamalla bioluminesenssia.

Tulosten perusteella DNA-origamia voidaan käyttää kuljettamaan entsyymit solun sisään, ja entsyymit säilyttivät aktiivisuutensa transfektion jälkeen. Lisäksi kompleksin entsyymikinetiikkaa voidaan mahdollisesti kontrolloida säätämällä polymeerien määrää päällysteessä. Entsyymi ei kuitenkaan sitoutunut spesifisesti origamiin, ja origamin muoto ei näyttänyt vaikuttavan transfektion tehokkuuteen. Kompleksin stabiilisuutta ja eheyttä on tutkittava tarkemmin.

Avainsanat: DNA-origami, DNA-nanoteknologia, lääkeainekuljetin, Streptavidin-Lucia luciferase -entsyymi, *in vitro*

Preface

The work behind this thesis was carried out in the Biohybrid Materials Group at Aalto University in the School of Chemical Technology. First, I would like to thank Professor Mauri Kostiainen for the opportunity to join the group and for supervising my thesis. I am also grateful for my advisor Veikko Linko for his guidance throughout the thesis. In addition, I would like to thank Ari Ora for performing the cell culture studies and Jenny Kiviaho for providing the polymer samples.

Finally, I want to thank my family and friends for their support. Especially, I would like to thank Henni for our friendship during the six years of my studies and for being supportive of my thesis work. Thanks also to my sister and Antti for their encouragement and help.

Otaniemi, 25.3.2016

Erika Järvihaavisto

Contents

Symbols and abbreviations

Symbols

A	absorbance
β	stretching exponent
I	luminescence intensity
l	length of light path
T	time constant
ε	extinction coefficient

Abbreviations

ATM	atomic force microscopy
bp	base pairs
CCMV	cowpea chlorotic mottle virus
CP	capsid proteins
CpG	cytosine-phosphate-guanosine
DNA	deoxyribonucleic acid
dsDNA	double-stranded DNA
ssDNA	single-stranded DNA
DMEM	Dulbecco's modified Eagle's medium
DNO	DNA nano-octahedron
DOX	doxorubicin
EDTA	ethylenediaminetetra acetic acid
ERT	enzyme replacement therapy
EthBr	ethidium bromide
FBS	fetal bovine serum
FRET	fluorescence resonance energy transfer (analysis)
GOx	glucose oxidase
HEK293 cells	human embryonic kidney cells
HRP	horseradish peroxidase
LSDs	lysosomal storage diseases
LUC	Streptavidin-Lucia luciferase
MDa	megadalton
NMR	nuclear magnetic resonance
NTV	neutravidin
PBS	phosphate-buffered saline
PDMAEMA	poly(2-dimethylamino)ethyl methacrylate
PEG	poly(ethylene glycol)
PEGylated	polyethylene glycol conjugated
PEI	polyethylenimine
PFA	paraformaldehyde
qPCR	quantitative polymerase chain reaction
rcf	relative centrifugal force

RNA	ribonucleic acid
mRNA	messenger RNA
siRNA	small interfering RNA
STV	streptavidin
TEM	transmission electron microscopy
Tris	tris(hydroxymethyl)aminomethane
UV/VIS	ultraviolet/visible (spectrophotometry)
2D	two dimensional
3D	three dimensional

1 Introduction

DNA nanotechnology is a rapidly growing research field whose aim is to construct nanoscale structures and functionalized materials from DNA. This has broadened the concept of DNA and today it is not only a biomolecule that carries genetic information. The field of DNA nanotechnology was pioneered in 1982 by Nadrian Seeman who designed rigid branched DNA motifs based on the complementary Watson-Crick base pairing [1]. Since then, the field has grown significantly and various complex artificial two- and three-dimensional (2D and 3D) DNA nanostructures have been fabricated for different functions and applications. Figure 1 illustrates the development of DNA nanostructures from linear one-dimensional structures to more complex nanometer-scale objects. One of the most common method to fabricate DNA nanostructures is known as a scaffolded DNA origami. In this method, a long viral single-stranded DNA is folded into a desired shape with the help of short synthetic oligonucleotides. DNA nanostructures have been studied for various applications, including nanoelectronics, single-molecular recognition, analyze of chemical processes and medical applications.

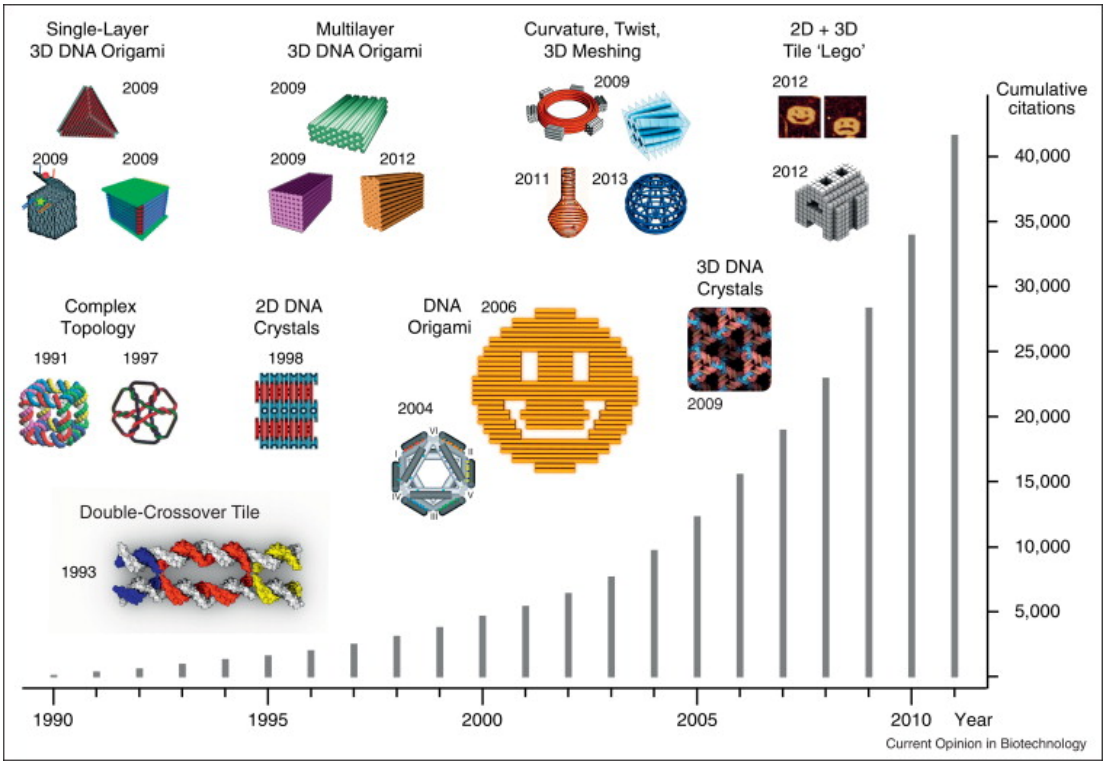

Figure 1: The interest towards structural DNA nanotechnology has grown enormously in recent years. Various self-assembled 2D and 3D DNA nanostructures have been developed for multiple functions. [2]

The development of DNA nanotechnology offers new possibilities for developing drug delivery nanocarriers. Drug delivery systems have been developed to protect drugs from degradation in physiological environments and reduce their side effects by improving their targeting efficiency to specific cells. The current clinically approved

nanotechnology drug delivery systems are quite simple. Therefore, nanocarriers with more complex properties, such as cell targeting and triggered drug release properties, are needed. Various drug delivery systems have already been demonstrated using organic nanomaterials, such as liposomes and cationic dendric polymers, or inorganic nanomaterials, such as gold nanoparticles and carbon nanomaterials. However, these nanomaterials can be toxic when implanted. [3] Instead, DNA nanostructures are purely biomolecules, which makes them biocompatible with biosystems. DNA nanotechnology enables control over size, shape and functionality of drug delivery systems. Especially a DNA origami is a promising candidate to be used as a nanocarrier, since its folding process is simple and any desired functionality can be added to it with nanometer precision. In the future, these DNA origami nanocarriers could be possibly utilized in various therapeutic applications, e.g., cancer therapy, prodrug medication and enzyme replacement therapy. [4]

The aim of this thesis is to use a DNA origami nanocarrier for the delivery of active enzymes into cells *in vitro*. Various DNA structures loaded with specific molecules have been managed to deliver into cells *in vitro* and *in vivo*. However, only a few studies that concentrate on the activity of enzymes in cells have been published [5]. Therefore, this thesis also examines the ability of enzymes to retain their activity after transfection into cells. In addition, the origami nanocarriers were coated with various polymers, and the effect of these coatings on the enzyme activity is investigated.

Chapters 2–4 form the theoretical part of this thesis. First, the structure and properties of DNA are described for facilitating the understanding of DNA origami construction. One of the most important properties for drug delivery systems are biocompatibility and biodegradation, therefore these properties of DNA are discussed in more detail. Chapter 3 provides an overview of DNA origamis. Folding method of DNA origami and some examples of single-layer and multi-layer origamis are presented. In addition, the possible applications of origamis are discussed. Chapter 4 focuses on DNA origamis as cellular delivery vehicles. Chapter 5 describes the materials and methods required for the fabrication of DNA origami nanocarries loaded with enzymes. Chapter 6 presents the results from the transfection studies and the enzyme activity measurements that were performed using a bioluminescence assay.

2 DNA nanostructures

Deoxyribonucleic acid (DNA) has gained a great attention as a building material because of its distinctive properties. The most important property is the highly recognition between two complementary DNA nucleotides due to the Watson-Crick base pairing. The second property is that the nanoscale structure of DNA is well-understood, therefore the rigidity and flexibility of DNA can be easily tailored. The second property is that DNA can be easily synthesized, modified and replicated. The final property is that DNA is a nontoxic and biocompatible material, which makes it suitable for a wide range of applications. [6, 7] In this chapter, the structure and properties of DNA are discussed in more detail.

2.1 Structural properies of DNA

DNA is a biopolymer build from deoxyribonucleotide units. Each nucleotide is composed of a phosphate-deoxyribose backbone and a nitrogenous base, as can be seen in Figure 2a. DNA contains four different bases: adenine (A), guanine (G), cytosine (C) and thymine (T). These bases are derivates of purine or pyrimidine. Deoxyriboses are sugars that are linked together by phosphate groups that form a phosphodiester bridge between the 3'-hydroxyl of the sugar of one nucleotide and the 5'-hydroxyl of the adjacent sugar. The base sequence is written in the 5' $\rightarrow$ 3' direction. The structure of a base bonded to a sugar is called nucleoside, whereas nucleotide is a phosphate ester of a nucleoside. A DNA chain is polar because of 5'-OH and 3'-OH groups in the end of the chain. [8, pp. 74–83] In addition, DNA chain possess a negative charge, since the phosphate groups (PO_4^-) in the backbone are negatively charged [9, pp. 11].

DNA molecules can be single-stranded (ssDNA) or double-stranded (dsDNA). Two complementary ssDNA strands can be joined together by hydrogen bonds between pairs of bases, thus forming a dsDNA double helix structure. The structure of a double-helical DNA is shown in Figure 2b. The base paring follows the Watson-Crick base-paring rule: adenine is always paired with thymine and guanine with cytosine. [8, pp. 74–83] The attraction between guanine and cytosine is stronger because guanine forms three hydrogen bonds with cytosine with an energetic stabilization of hydrogen bonds of about $E_{G-C} = 11$ kcal/mol, whereas adenine forms only two with thymine with a stabilization energy of $E_{A-T} = 6.0$ kcal/mol [10]. For that reason, the more G-C pairings DNA double helix contains, the more stable it is against heating and pH change. [8, pp. 86]. The interactions between base pairs are quite weak in contrast to the covalent bonds, for example the strength between two carbon atoms is $E_{C-C} = 83.1$ kcal/mol [9, pp. 273]. Because of relatively weak interactions between base pairs, the double helix can be denatured into two single strands by heating or exposure to high pH or low salt concentration. Thus the process is reversible. [8, pp. 74–83] The Watson-Crick base paring is the most favored type of interaction between DNA strands because of hydrogen-bonding requirements and steric factors [6]. In addition to hydrogen bonds, the stability of a double helix is affected by other interactions, such as base-stacking interactions, electrostatic

forces and hydrophobic interactions [7, 11]. Base stacking interactions consist of van der Waals and dipole-dipole interactions between adjacent bases in a double-helical structure. DNA is soluble in water, which also stabilizes the structure of a helix [12].

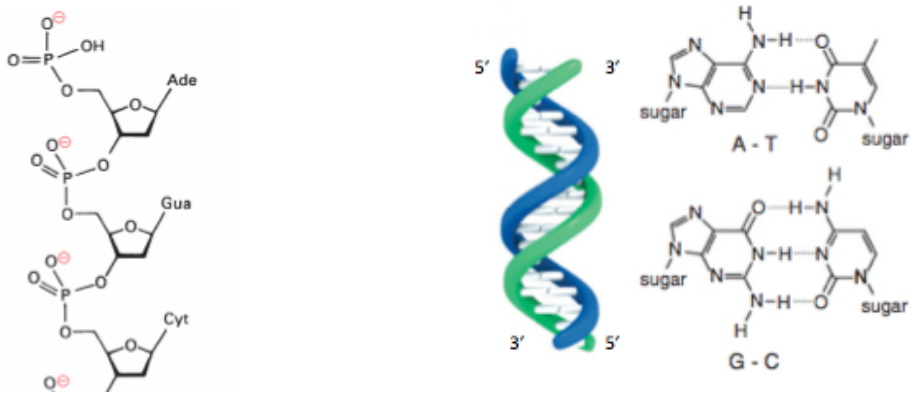

(a) (b)

Figure 2: (a) Negatively charged sugar-phosphate backbone with adenine, guanine and cytosine bases [12]. (b) DNA double helix structure is formed by the Watson-Crick base pairing rule: adenine is paired with thymine and guanine with cytosine. Adapted from [6].

Two DNA helical chains are coiled around a same axis and they run in opposite directions, which signifies that the formed double helix is anti-parallel. The bases are on the inside of the helix and perpendicular to the main axis, while the phosphate and deoxyribose units are on the outside of the helix. [8, pp. 74–83] The dimensions of a DNA double helix are on the nanoscale. The helix has a diameter of about 2 nm and a helical periodicity of 10-10.5 nucleotide pairs per turn that is about 3.5 nm per turn [6, 13]. Usually, the length of a DNA strand is informed in base pairs (bp). DNA double helices are fairly rigid polymers when their length is below 50 nm that is 150 base pairs. By contrast, single stranded DNA is much more flexible. Combining these two different strands, it is possible to construct staple motifs with desired geometry. [6]

DNA can form different kinds of helical structures, including B-DNA, A-DNA and Z-DNA conformations. B-DNA is the most abundant DNA conformation under physiological conditions. Its helical chains consist of 10.5 base pairs per full turn (360°), whereas the helical periodicity of A-DNA is 11 bp per turn and that of Z-DNA is 12 bp per turn. B-DNA and A-DNA are right-handed double helices, while Z-DNA is left-handed as seen in Figure 3. B-DNA can turn to A-DNA due to dehydration. [8, pp. 815–816] Different base sequences in B-DNA structure influence helical twist, mechanical ridigity and resistance to bending of a double helix [12]. There are also other more uncommon conformations, such as triple-stranded DNA and four-stranded motifs called tetraplexes [14]. In the examples of this thesis, DNA is in conformation of B-DNA.

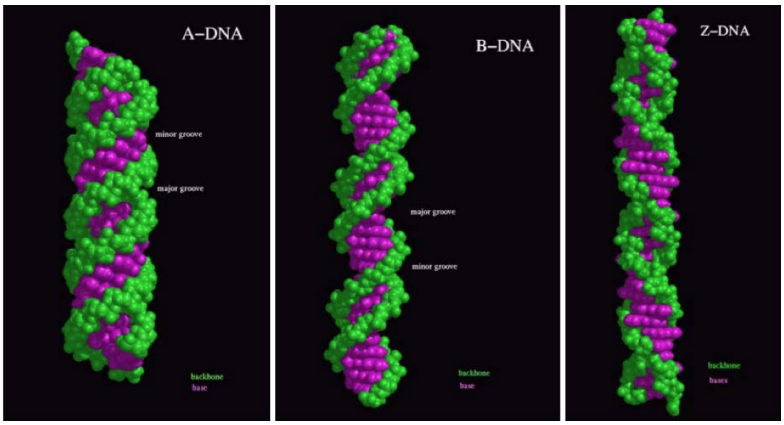

Figure 3: DNA can adopt different conformations, such as A-DNA, B-DNA and C-DNA. Most of the DNA are in the B-DNA form in physiological conditions. The color violet and green signify the bases and the backbone of DNA double helix respectively. [11]

DNA nanostructures form spontaneously via base pairing interactions of complementary DNA strands in a process called self-assembly. In other words, DNA single strands can spontaneously hybridize together to form a double helix. The shape and functions of DNA constructs are encoded in the sequences of the constituent nucleic acid molecules. Hence, DNA strands are highly programmable structural building blocks. The simplest DNA constructs can be formed by hybridizing two dsDNA that have complementary single-stranded extensions ('sticky ends') at the end of the helix. In order to achieve more complex structures, branched DNA motifs have been combined with sticky-ended cohesion. [13] This construction method has been used to build periodic structures, such as two- and three-dimensional crystals [15, 16]. The four-arm branched DNA molecule is one of the simplest examples of branched structures [17]. Figure 4 shows a branched four-arm junction that forms a larger complex with sticky-ended cohesion. Besides crystal structures, DNA can be used to construct large objects by DNA origami method that is discussed in Chapter 3.

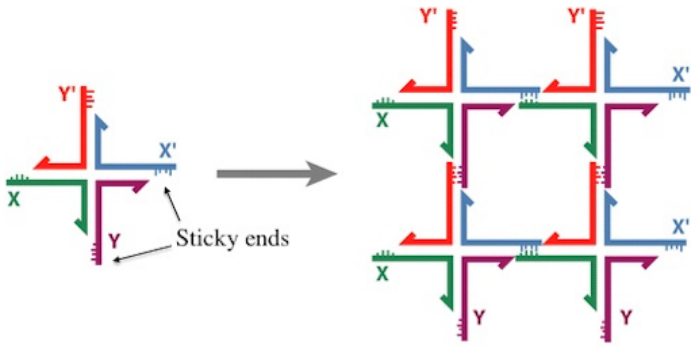

Figure 4: The four-arm branched DNA molecule forms a larger arrangement by self-assembly. The DNA branched junction consist of four DNA strands with sticky ends. The complementary sticky ends (e.g., blue and green strands or red and purple strands) associate together and form a quadrilateral structure.[15]

Oligonucleotides can be conjugated with a wide variety of materials, including proteins, dyes, metal nanoparticles or other small biomolecules. For example, DNA oligonucleotides can be covalently modified with biotin groups which can bind to streptavidin protein [18]. Functionalization of DNA enables to organize biomolecules or nanoelectronic and nanophotonic components in a nanoscale precision. Figure 5 shows two-dimensional DNA arrays that is used to organize gold nanoparticles. Two different triangle shaped motifs are connected with sticky-ends to form a larger array, and gold nanoparticles with a size of 5 nm or 10 nm are attached to the structure [19]. It is also possible to construct multifunctional DNA nanostructures, since different arms of multibranched DNA nanostructures can be decorated with different functional groups.

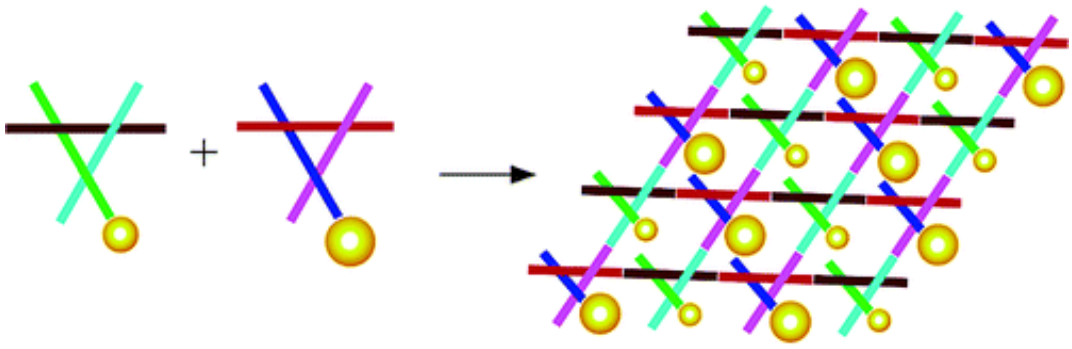

Figure 5: The 2D arrays for organizing gold nanoparticles. Two different triangle motifs are attached by 5 nm or 10 nm nanoparticles. The motifs are assembled to form a two-dimensional array. [19]

2.2 Biocompatibility and biodegradation of DNA

DNA nanostructures possess a great potential to be used in many biomedical applications, for example as nanocarriers for drug delivery. For that reason, it is important to ensure that DNA nanomaterials do not trigger toxic side effects and investigate the stability of these materials in physiological conditions. Nucleic acids are not toxic to cells, as they are found naturally in living organisms [20]. Several studies [21, 22, 23] have shown that DNA nanostuctures, such as DNA tetrahedron and DNA origami structures, have no effect on cell viability *in vitro*. For example, triangular and tubular DNA origami structures did not show any cytotoxicity to cells after 48 h of incubation [22]. Furthermore, DNA nanostructures, such as DNA origami [24] and DNA tetrahedral nanoparticles [25], have proved to be biocompatible in *in vivo* studies. Zhang *et al.* [24] investigated a triangle-shaped DNA origami as an *in vivo* delivery vehicle for cancer therapy. This DNA origami nanocarrier did not induce observable systemic toxicity in nude mice. In addition, the blood analysis data from mice treated with DNA origamis for 6 h did not differ from normal values.

DNA is degraded unselectively by nuclease enzymes *in vivo* [20]. These enzymes break up the phosphodiester linkages in the DNA backbone. However, DNA nanostructures in contrast to DNA have shown to be more resistant to nuclease

degradation. A DNA tetrahedra structure [26, 21] and DNA origami objects [27] have proved to degrade slower than a linear DNA structure. Mei *et al.* [28] revealed that different DNA origami structures are stable in various cell lysates for at least 12 h at room temperature, in contrast to natural, single- and double-stranded DNA that were susceptible to degradation after 1 h of incubation. DNA origami structures maintained also their functionality after exposure to cell lysates. Mei *et al.* suggested that the better stability of these DNA origami structures in cell lysates might result from the rigidity, compact organization and the high negative charge density of the structure.

Hahn *et al.* [29] examined whether *in vitro* tissue culture conditions cause denaturation of DNA origami nanostructures. They concluded that physiological cation concentrations of cell culture medium are too low for keeping DNA structures stable. The sensitivity to low cation concentrations depends on the design of DNA structures and time: only one of four tested structures, DNA nanotube, remained stable after 24 h at 37 °C. By increasing the cation concentrations of the media, denaturation of all the tested structures was prevented with only a little impact on cell viability. In addition, the denaturation of DNA structures is caused by nucleases present in fetal bovine serum (FSB) used as a medium supplement. Addition of 10 % FBS to the medium caused great degradation of the structures by 24 h. The activity of nucleases could be inhibited by using actin protein as an inhibitor in a cell culture medium. The stability of the DNA structures were analyzed by agarose gel electrophoresis and transmission electron microscopy (TEM). [29] Moreover, Benson *et al.* [30] noticed that the structures with more open conformation could withstand cell culture buffers better than more dense structures. In another study [31], the stability of DNA nanostructures in live cultured mammalian cells was examined using fluorescence resonance energy transfer (FRET) analysis. FRET analysis is sensitive to the distance between a pair of fluorophores labeled on DNA structures. The study revealed that DNA cages remained intact within the cells for at least 48 h after transfection. [31]

The stability of oligonucleotides can be enhanced via chemical modifications of DNA or by covering DNA with lipid bilayers. Recent study [32] has shown that nuclease resistance can be enhanced by introducing simple chemical modifications to oligonucleotide ends with hexaethylene glycol and hexanediol groups. Unmodified and modified DNA strands were used to construct DNA cages, and the stability of these structures were evaluated in 10 % (v/v) FBS which contains a mixture of nucleases and proteins. The DNA cage containing end-modifications showed increased nuclease resistance with the lifetime of 62 h. In addition, this DNA structure possessed greater stability than its modified components strands alone. Perrault *et al.* [33] suggested that stability of oligonucleotides could be enhanced by encapsulation of DNA nanostuctures by lipid bilayers. This method is inspired by viruses that maintain structural integrity by encapsulating their genome and protein capsid shell in lipid envelope. In this study, a wireframe DNA nano-octahedron (DNO) structure that resembles a viral protein capsid shell was designed and it was enveloped by PEGylated (polyethylene glycol conjugated) lipid bilayers. The more lipids were attached to DNA structure, the more protection it provided against

nuclease enzymes, such as DNase I digestion. Moreover, the injection of encapsulated DNO and non-encapsulated DNO into mice showed that encapsulation improves the pharmacokinetics properties of DNO and decreases immune activation. DNA could also be covered with virus capsid protein (CP) itself, which was found to improve the delivery of origamis into cells and be biocompatible with cells [34].

3 DNA origamis

A DNA origami method was introduced in 2006 by Paul Rothemund [35]. He discovered that DNA origami structures could resolve the problems associated with other methods that use short complementary oligonucleotides to construct large DNA nanostructures. The problems with the other methods, such as with a multistranded approach, are due to multiple purification steps of oligonucleotides, low yields of product and strict stoichiometry control. For that reason, these methods are limited to construct only simple geometric shapes. [35, 36] In the DNA origami method, a long single stranded DNA called 'scaffold' is folded into desired shapes with the help of multiple short single-strands of DNA called 'staple strands'. Scaffolded DNA origami method has fewer defects and higher yield than other assembly methods. In addition, by using DNA origamis more complex nanoscale shapes can be created, and its dimensions can be precisely controlled. The folding of DNA origamis is also quite simple and synthesis times are reduced, as there is no need for stoichiometry control or multiple purification steps of oligonucleotides. [37] DNA origamis can be fold into a wide variety of structures ranging from simple 2D and 3D lattices to complex 3D shapes. The structures can be easily functionalized by integrating functional groups to staple strands, which allows attachment of e.g. chemical groups, biomolecules or fluorescent dyes to the structure. This enables the use of DNA origamis in a wide range of applications. DNA origami method and multistranded approach are compared in Figure 6.

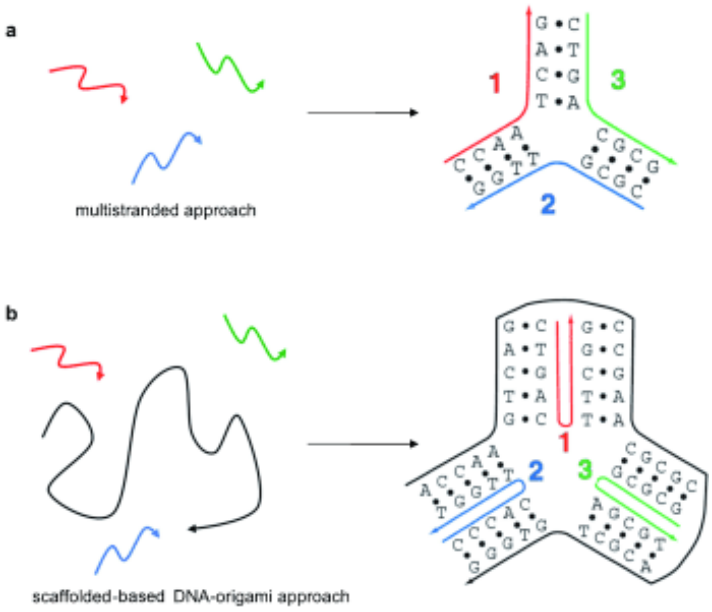

Figure 6: (a) The multistranded approach uses short complementary single strands to assemble into a branched DNA motif. These motifs can form larger structures by sticky-ended cohesion. (b) In the DNA origami approach, a long single stranded scaffold forms base pairs with multiple short single strands, which leads to a desired shape. [36]

3.1 Folding of DNA origami

A long single-stranded scaffold is usually taken from the circular M13mp18 bacteriophage genome while staple strands are synthetically produced. The M13mp18 scaffold is about 7000 nucleotides long and it can form structures with tens to hundreds nanometer dimensions with a molecular weight in the megadalton (MDa) region [38]. It is also possible to use other types of scaffold strands, such as smaller scaffolds [39] or scaffold strands from double-helical DNA [40]. Typically a few hundred staple strands are needed to form DNA origami, for example Rothemund used over 200 staple strands to fold the M13mp18 scaffold into two-dimensional shapes with a spatial resolution of 6 nm [35]. The length of staple strands can vary from 18 nucleotides to 50 nucleotides. Strands below 18 nucleotides may not be stable at room temperature and strands over 50 nucleotides may not be sufficiently pure. The long continuous single-stranded scaffold forms the shape of a desired object. Staple strands bond to scaffold by the Watson-Crick base pairing, hence scaffold sequences determine the sequences in the staple strands. In addition to double-helical domains, DNA origami structures can also contain single-stranded domains which can for example prevent base-stacking interactions between interfaces or act as an attachment site for other molecules. [27]

In order to form a desired shape, double-helical domains must be connected to adjacent double-helical domains by antiparallel interhelix cross-overs. These cross-overs are positions at which strands running along one helix switch to an adjacent helix and continue running there, as shown in Figure 7a and 7b. The position of cross-overs depends on the desired packing lattice. 2D and 3D DNA origami structures have different packing lattice rules that are discussed in more detail in the next section. The structure of DNA origami and the positions of cross-overs can be easily designed by using computational tools. The software caDNAno facilitates designing and analyzing the structure of DNA origami [41]. caDNAno files can be analyzed by the computational tool called CanDo [27]. It analyzes the shape of desired object: bending, twisting and rigidity.

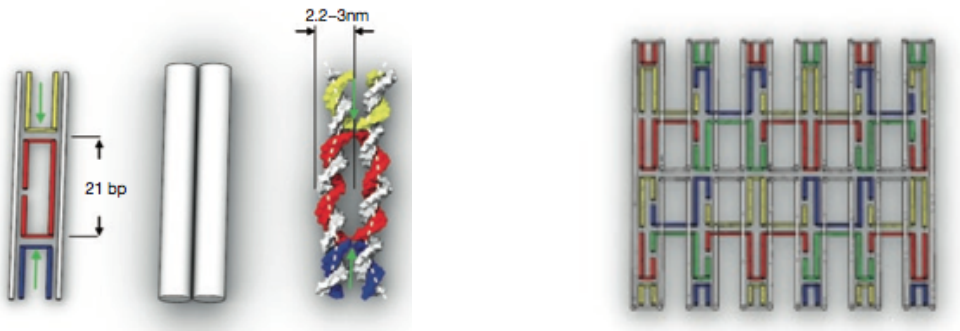

(a) (b)

Figure 7: (a) Stable strands (coloured strands) forming cross-overs every 21 base pair to the adjacent DNA scaffold strand (white strand). (b) Scaffold forms the desired structure with the help of multiple staple strands. Adapted from [27].

Staple strands can bind to incorrect places on the scaffold. However, there are excess amount of staple strands in the reaction solution which can correctly bind and displace incorrect strands. This is called as a strand invasion. Different staple strands can also interact with one another but there is no perfect complementary base-pairing between them as there is with the scaffold and the staple strands. For that reason, the stoichiometry between staple strands has no importance. The excess of staple strands also prevents the scaffold from forming secondary structure by itself. [35]

The first step for building DNA origami objects is to design and analyze the desired structure with caDNAno and CanDo programs and decide the lattice packing rule. The design of 3D objects requires more accurate theoretical optimizations than 2D objects. In the folding process, staple strands and a M13mp18 scaffold are mixed in a fixed stoichiometry with the existence of cations, water and pH stabilizing buffer. Cations are needed to prevent the negative charge-repulsion forces of the nucleic acid phosphodiester backbone. Cation concentrations in the reaction solution depend on the structure of a DNA origami, for example 3D structures require more cations than 2D structures. The mixture is exposed to a thermal denaturation and annealing procedure during which the folding of a DNA origami occurs. Denaturation occurs by heating the mixture to about 70–80 °C, and then the mixture is cooled down slowly. [27] The structure of origamis determines the temperature at which DNA origamis are folded. Multilayer DNA objects are detected to fold at temperatures between 45–60 °C [42]. Single-layer objects can self-assemble within few hours. Multilayer objects usually require several days to self-assemble but complex objects have also been succeeded to fold in less than an hour [42]. The assembly reaction conditions should reach a minimum energy state when the target structure is self-assembled.

After the folding, DNA origami objects are purified from the excess staples. Purification methods include ultrafiltration, gel filtration with spin colums, agarose gel extraction, poly(ethylene glycol) (PEG) precipitation or ultracentrifugation [43]. The selection of the most suitable purification method depends on the functional groups attached to origamis and the target application. The quality of folding and purification of DNA origamis can be detected by agarose gel electrophoresis. DNA origamis can be imaged with atomic force microscopy (AFM) and negative-stain or cryogenic transmission electron microscopy (TEM).

3.1.1 Single-layer DNA origami

One of the first examples of single-layer origamis were Rothemund's star, smiley face, rectangle and triangle origamis with a diameter of about 100 nm [35], as shown in Figure 8. These structures are synthesized in less than two hours and the highest yield obtained was 90 %. In order to achieve planar structures, cross-overs in one helix should occur every 1.5 helical turns (16 bp) to two adjacent double-helices, which means that the interhelical connections are formed every 180° along alternating sides of a helix.

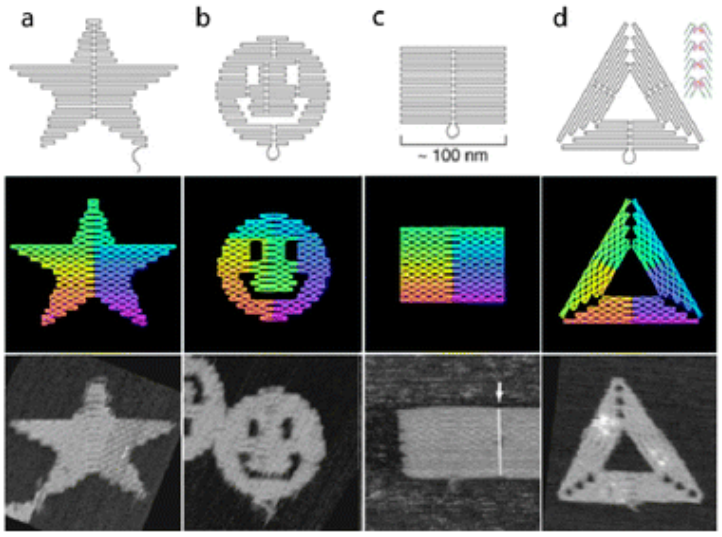

Figure 8: Single-layer DNA origami shapes: (a) star (b) smiley face (c) rectangle (d) triangle. Top row presents the scaffold routing. Second row shows the base-pair index along the folding path: red is the 1st base and purple the 7000th. Bottom row shows AFM images of the structures. [44]

The length of the scaffold determines the size of a DNA origami object. For that reason, various methods have been developed to construct larger 2D structures. One method to assemble larger structures is to use more complex staples. Zao *et al.* [45] scaled up the size of 2D DNA origami by using nine rectangular-shaped DNA tiles as staple strands instead of short oligonucleotides. They compared the size of origamis built from staple tiles with origamis built from short staple strands. A segment of M13mp18 scaffold of the same length was used to fold these origamis. The results showed that with staple tiles the size of the 2D DNA origami was increased from 34 nm x 28 nm to 54 nm x 70 nm. It is also possible to use DNA origamis as single tiles to fold a scaffold strand. This is called as an origami of origami or a superorigami. [45] In other study, Zao *et al.* [46] managed to create different superorigami structures from DNA origami tiles folded with pre-formed scaffold frames. These structures could broaden the size of origamis to micrometer scale. Another method to expand the size is to use double-stranded genomes as scaffolds. Yang *et al.* [47] used double-stranded DNA scaffold to fabricate DNA origami triangular structure that contains both of the constituent ssDNA molecules. The edges of the triangular structure fabricated were 215 nm. It is much larger than the maximum area and volume of an M13mp18 DNA origami structure that is 78 x 78 nm^2 for 2D and 24.7 x 24.7 x 24.7 nm^3 for 3D [47]. In addition, larger structures can be created by connecting individual origami tiles through sticky-ends association [48].

3.1.2 Multilayer DNA origami

Single-layer origamis cannot withstand very well mechanical stress and their structures are quite simple [36]. As a result, more complex and rigid 3D origamis have been developed. Douglas *et al.* [49] were the first to design DNA origami objects with 3D

structures. They successfully designed six different 3D DNA origami shapes with dimensions ranging from 10 nm to 100 nm. Since then, various different 3D structures have been developed, such as a hollow box, tubular and triangular structures and a nanoflask structure. Figure 9 presents different 3D origami structures.

Two main strategies are used to build three-dimensional DNA origamis. In the first method, individual single-layer origami sheets are interconnected at the edges by joint strands to form hollow 3D cages, such as a hollow box as shown in Figure 9a [50]. The second method utilizes cross-overs to interconnect antiparallel helices, which allows to construct more densely packed structures. The packing rule can be a honeycomb or square lattice. In the honeycomb lattice, cross-overs are formed every 7 bp, which means the rotation of 240° in the helical axis and cross-overs every 21 bp are formed to the same adjacent strand (Figure 9c). [27] As shown in Figure 9e and 9f, cross-overs that are not formed every 7 bp in the selected array of honeycomb lattice packing cause twisting of the target object. Moreover, deleting of one base pair on one side of array and inserting one base pair on the opposite side of array cause global bending of the helices (Figure 9g). The degree of the curvature could be fine-tuned by varying the number of insertions and deletions of base pairs. [51] DNA origami can also be packed into a square lattice. In the square lattice packing, cross-overs are placed to four nearest neighbor strands, which leads a more dense structure (Figure 9d) [27].

Various examples of three-dimensional DNA origamis with twisted and curved structures have been reported. Han *et al.* [52] designed curved DNA origami structure with Möbius topology. Möbius strip means a strip with a half-twist that is joined together at the ends of the strip to form a loop. The strip contained eleven DNA double helices and it was 210 nm in length and 25–30 nm in width. In the later study, Han *et al.* [38] created a method to construct more complex DNA origamis with curved surfaces (Figure 9b). They succeeded to assemble 2D concentric rings, 3D spherical shells and spheres and nanoflasks. Different curvatures were created by increasing the number of base pairs between crossovers of the adjacent helices so that the distance between the crossovers increases from inner to outer circles. In addition, designing helices with less or more than 10.5 bp per helical turn induced global twisting.

The mechanical stability of 3D DNA origamis can be improved by tensegrity structures. Tensegrity is a concept that refers to a discontinuous set of compression elements that are opposed and balanced by a continuous tensile force. The balance between the two forces leads to stable and mechanically rigid structures. [36] Liedl *et al.* [53] designed a 3D tensegrity prism composed of three compression-resistant bundles of DNA double helices that was held in place by tensed single-stranded DNA segments (Figure 9c bottom). They proposed that by using a single-stranded DNA as a source of tensile force in DNA structures, it could be possible to construct more flexible and mechanically responsive DNA structures. These structures could be used to study molecular forces and other biological processes.

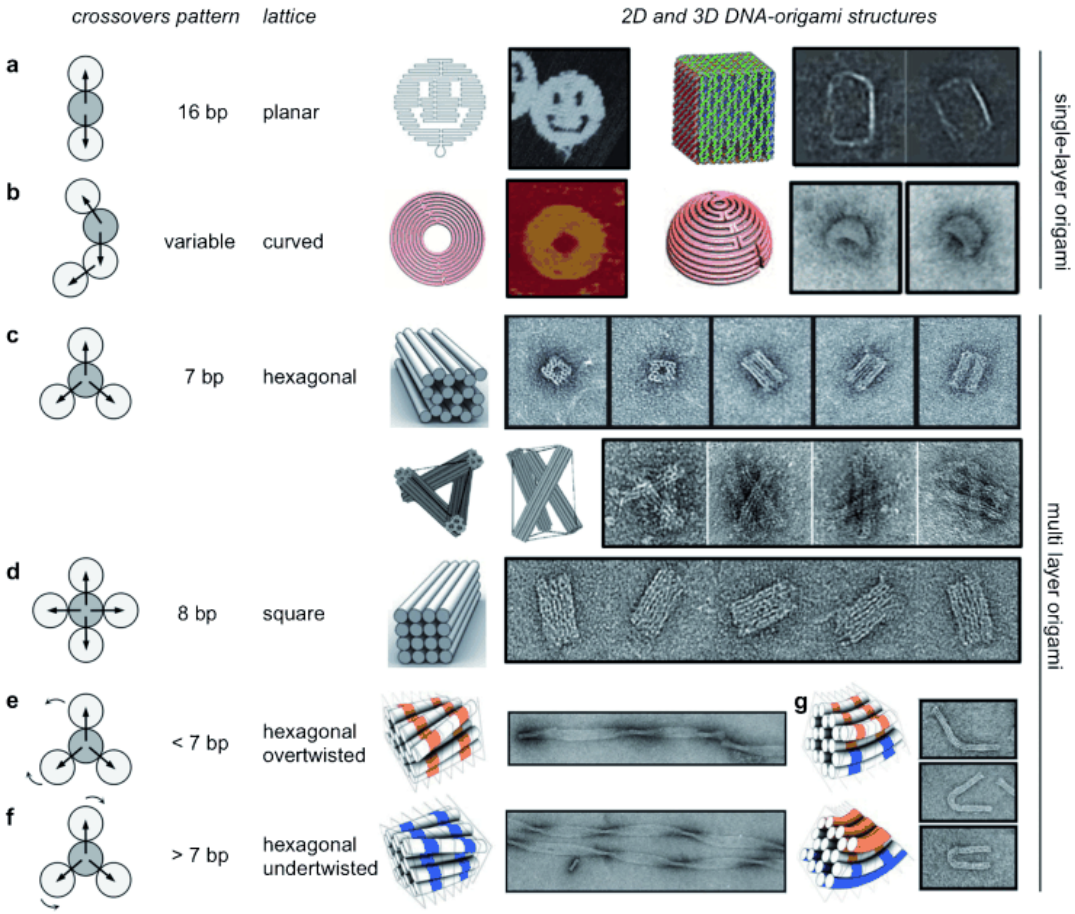

Figure 9: Different kinds of spacing rules and the resulting 2D or 3D structures of DNA origami. The second column presents the number of base pairs between cross-overs along the same helical axis. (a-b) shows single-layer and (c-g) multilayer DNA origami structures. [36]

3.1.3 Scaffold-free "origami" and meshing methods

In addition to scaffolded DNA origamis, scaffold-free designs have also been reported. In a scaffold-free method, desired 2D or 3D structures are constructed by hundreds of short synthetic single DNA strands called "tiles" or "bricks". Synthetic single-strands self-assemble into target structures by forming sticky-ends between different strands, therefore there is no need for the scaffold strand. Single strands can also be added or removed independently. [54] Ke *et al.* [54] constructed a cubic-like molecular canvas from DNA bricks of 32 nucleotides long with four 8 nucleotide binding domains. The canvas consists of cubes (voxels) and each voxel represents 8 bp interactions between bricks. By selecting subset of bricks from this canvas, one can create hundreds of different lego-like shapes. Figure 10a shows one example of lego-like shapes.

Other complex DNA nanostructures can be created *via* 3D meshing methods. Han *et al.* [55] managed to construct gridiron-like DNA origamis ranging from 2D structures to 3D structures and curved objects as shown in Figure 10b. The basic components of DNA origami gridirons are a long scaffold strand and four-arm

junctions built from short DNA strands. In their design, four-arm junctions were used as vertices and a scaffold strand was required to force the junctions to rotate and achieve the intended structure. The scaffold strand can travel through vertices in multiple directions. The shape and size of gridiron structures can be tailored by varying the length of individual junctions. In other study, Benson *et al.* [30] designed an algorithm to construct 3D DNA polygon meshes. The aim of the algorithm is to find a routing for a scaffold so that the scaffold forms a mesh by traversing the edges of the mesh only once. Moreover, the algorithm uses staple strands to connect the edges of the mesh as shown in Figure 10c, and it calculates also the physiological model in order to obtain more relaxed structure. Designed structures have more loose structure than conventional DNA origami structures that are built from close-packed helices. Benson *et al.* suggested that their method might enable rapid 3D printing at the nanoscale because of its highly automated design process.

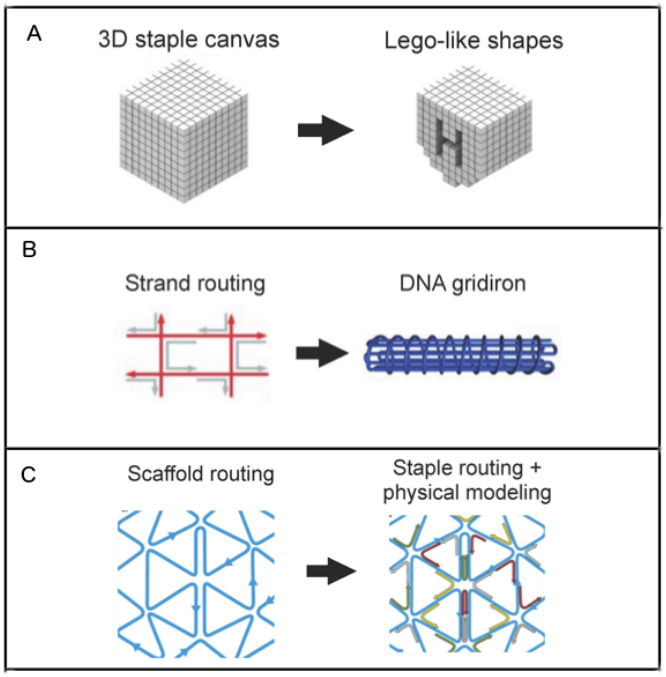

Figure 10: (a) Scaffold-free origami design. (b) and (c) 3D meshing methods to create complex DNA nanostructures. Adapted from [4].

3.2 Applications

One of the most important properties of DNA origami are the easiness of chemical modifications to its structure and the precise spatial control of functionalities attached to it. As a result, DNA origami nanostructures have gained a lot of interest in a wide range of applications. These applications include for example single-molecular recognition and arrangement, analyze of chemical and biochemical processes, nanoelectronics, molecular imaging and medical applications, including drug delivery systems and other complex tasks in cells. DNA origami-based drug delivery systems

are discussed in more detail in Chapter 4, while this chapter focuses on the other interesting applications of DNA origamis.

Since various techniques have been developed to chemically modify DNA oligomers, almost every functional group can be attached to DNA origami structures. Functionalization of DNA origamis can be attained by the hybridization of a modified DNA oligomer with a receptor connected to a staple strand or by directly using a modified DNA strand as a staple strand [56]. DNA origami structures have been conjugated with metal nanoparticles, carbon nanotubes, quantum dots and virus capsids, for instance [44]. One widely used chemical modification is the biotinylation of staple strands, which allows streptavin or avidin molecules to bind to the origami structure at selected positions. Biotin binding to avidin protein is one of the strongest known noncovalent interaction. The biotin-avidin interaction in origami structures enables conjugation of other biotinylated molecules with DNA origami, for example biotin-streptavin interaction has been used for the assembly of proteins on the origami surface [57]. As staple strands can be easily functionalized and they have an unique position within the origami structure, DNA origamis are promising platforms for arranging and recognizing objects with nanometer scale precision. For example, a nanoparticle-conjugated staple strand can hybridize with M13mp18 scaffold that position the conjugate to the target place [44]. Functionalities placed on the surface of 2D DNA origami can act as a probe for molecular recognition [58].

One of the first examples of molecular recognition using DNA origamis was the label-free detection of messenger RNA (mRNA) [59]. The DNA origami structure contained probe strands that were 20 nucleotides long single-stranded DNA segments. These probe strands selectively bound to the RNA targets. Three different probe strands were used to recognize mRNAs corresponding to regions of three different genes: *Rag-1, C-myc* or *β-actin*. It was noticed that the position of the probe affects target binding. According to this study, DNA origami may be used as a detector for gene expression at a single-molecular level. [59] Since then, DNA origami has been used for detection of many other molecules, for example it could be possible to detect single-nucleotide polymorphism [60] or conformational changes in DNA [61]. The single-nucleotide changes in the DNA code is the basis of genetic variation, and it can protect or alter some individuals to deseases, such as cancer or diabetes. Moreover, DNA origami method can be used for investigating the effect of the distance between adjacent probes on binding of the target substance, such as aptamer binding to protein [62].

DNA origami has also shown a great potential in studying dynamic processes, such as enzymatic reactions and molecular dynamics. Chemical reactions can be precisely controlled and optimized by the spatial arrangement of components. Chemical components could be arranged close to each other with DNA origami in order to fasten reaction rates, as illustrated in Figure 11a. DNA origami could also artificially direct enzyme cascade reactions by choosing the correct stoichiometry, and thus improving reaction flux. Three-dimensional DNA origamis could also mimic the closed enzyme assemblies in which components could be encapsulated by the origami structure (Figure 11b). Such systems could prevent diffusive loss of reaction intermediates to the bulk. Another possible approach to prevent loss by diffusion

is to use DNA-based motors to transport molecular components between reaction centers. With these properties DNA origamis could serve as nanofactories in future applications (Figure 11c). [63]

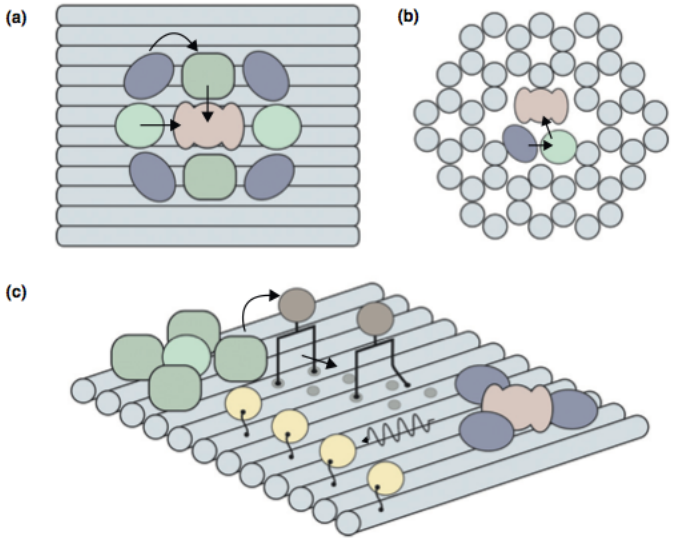

Figure 11: DNA origami (in grey) for controlling chemical reactions. (a) DNA origami could precisely control the placement of reactants to increase the reaction rate. (b) DNA origami could also encapsulate reactants to avoid diffusion of intermediates. (c) DNA origami-based nanofactory for performing several tasks. DNA walkers (in black) could transport reactants between reaction centers.[63]

DNA-based nanodevices that control chemical synthesis have also been reported. Gu *et al.* [64] presented a DNA-based assembly line that uses a DNA walker to fabricate different objects from gold nanoparticles. A DNA origami was used as a framework to which cargo-donating devices were attached. A triangle-shaped DNA walker with single-stranded DNA segments as hands and feet moved from device to device on the DNA framework and collected the gold nanoparticle cargoes. The cargoes and the devices were encoded with appropriate DNA sequences in order to the walker to recognize the correct attachment sides. DNA origami structures could also be used to investigate the properties of motor protein ensembles. Derr *et al.* [65] designed 3D DNA origami template with specific binding sites for motor proteins. The number of attachment sites for the proteins was demonstrated to affect the velocity of a single protein. They also noticed that the binding ability of a motor protein was dependent on the presence and number of other motor proteins. [65].

DNA origami-based hybrid materials have gained a great interest as a component in nanoelectronics, because they can arrange metal nanoparticles and other inorganic materials. Hybrid materials consist of two or more different constituents at nanometer or molecular level. The metallization of DNA with gold, silver, copper or nickel enables the formation of conductive elements for nanocircuits. However, the metallization of DNA origami presents several challenges, including the stability of the origami during metallization and more difficult surface adhesion due to the small size of

DNA origami. [66] For the potential use in nanocircuits, it is important to be able to precisely control the position and orientation of origami templates [44]. Hung *et al.* [67] combined top-down lithography and bottom-up DNA self-assembly to arrange 5-nm gold nanoparticles. The arrangement of these nanoparticles is not possible with conventional lithography methods, since only about 100 nm patterns can be obtained. AFM images (Figure 12) showed that gold nanoparticles attached to the corners of the triangular DNA structure that was bound selectively on the patterned silicon oxide surface of the substrate. The binding was performed by lithographic patterning in which negatively charged origami structures bound to hydrophilic patterns on hydrophobic surface. [67] Moreover, the position of origamis could be controlled by a dynamic dielectrophoresis [68]. Maune *et al.* [69] demonstrated also that DNA origamis can be used to organize single-wallet carbon nanotubes that have great electronic properties. Another study showed that the arrangement of metal nanoparticles by DNA origami can lead to chiral plasmonic structures with optical activity [70].

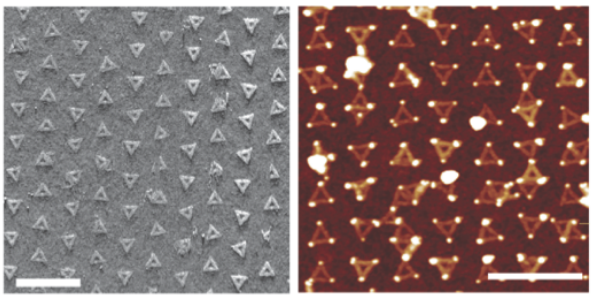

Figure 12: The adsorbed origami structures were imaged by AFM [67]. The left figure demonstrates the control over the position and orientation of triangular DNA origami templates by lithography patterning. The right image shows gold nanoparticles that were attached to the corners of origami templates. Figure from Ref [44].

DNA origami could also be used as a ruler to measure distances between single molecules, such as fluorescence dyes, and to calibrate superresolution microscopic techniques [71] that can be used in imaging objects below the diffraction limit of light of about 200 nm. Moreover, DNA origami is a promising platform for controlling the position of multiplexed fluorescent tags, therefore it could be used as *in situ* imaging probes for fluorescence microscopy [72]. Another possible application includes DNA origami for determination of the structure of membrane protein by nuclear magnetic resonance (NMR)[73].

4 Cellular delivery vehicles

DNA nanostructures are promising candidates to be used as nanocarriers in drug delivery systems for various therapeutic applications. As a result, multiple promising examples of DNA origamis and other DNA-based nanomaterials as nanocarriers have been reported, however it must be emphasized that the development of DNA delivery vehicles is in its early stage. In this chapter, the properties of DNA nanostructures that meet the most important requirements for delivery vehicles are discussed. In addition, several DNA-based nanocarrier systems are presented in order to understand the versatility of DNA as a nanocarrier for various cargoes. The final section describes more closely three potential therapeutic applications for DNA-based delivery vehicles that are enzyme replacement therapy, prodrug medication and anticancer therapy.

4.1 Requirements for delivery systems

Several requirements must be taken into account when designing cellular delivery vehicles. First of all, delivery vehicles must be biocompatible in cellular environment and biodegradable to minimize the risk of toxicity. Delivery systems should be able to be loaded with cargoes and protect them from chemical and enzymatic degradation. They must also remain stable in cellular environment until entering cells and releasing their cargoes. Highly desired properties also include the release of drugs in a controlled manner and selective recognition of target cells to achieve appropriate circulation times and to avoid side effects. [74, 20] Figure 13 illustrates some obstacles that delivery vehicles must overcome to obtain therapeutic effects.

Cellular environment affects the stability and the diffusion of DNA nanostructures. As a biological material, DNA nanostructures are biocompatible and biodegradable in cellular environments. However, several studies have demonstrated that DNA nanostructures can remain stable in cell culture media for 24 h [29] and even in cells for about 48 hours [31]. The stability and biocompatibility of DNA were already discussed in more detail in Chapter 2.2.

Nanocarriers should possess high loading capacity of cargoes, and their size should be precisely controlled. DNA nanomaterials can be designed into various architectures with a predictable and well-defined structure, which enables optimizing a variety of parameters for cellular delivery. For example, the position and spatial orientation of cargo molecules can be precisely controlled by DNA origamis. Various methods can be used for functionalization of DNA, including covalent modifications, biotin-avidin interaction, encapsulation of molecules into DNA structures and intercalation of molecules between planar bases of DNA. DNA constructs also enables multiple therapeutic molecules to be simultaneously incorporated and delivered, for example DNA nanostructures could be loaded with targeting ligands, anticancer drugs and therapeutic oligonucleotides [75]. The structures can also contain fluorescent dyes for detecting the targets. In addition, the density of conjugated molecules on the surface of DNA nanostructures can be well defined. [3] The density of surface molecules as well as the biophysicochemical properties of the vehicle, such as size, shape and charge, can effect on the circulation life and biodistribution of cargoes [76].

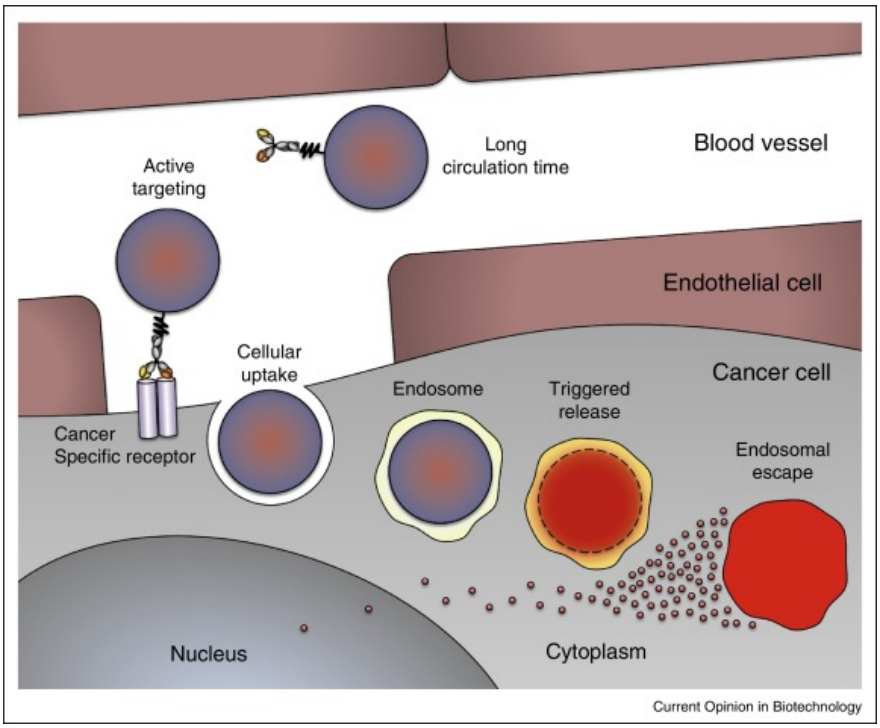

Figure 13: Some requirements that delivery systems must overcome to achieve therapeutic effects. These include long circulation time, active targeting, the ability to enter cells, to release of cargoes in a controlled manner and to escape from endosomes. [74]

Cellular delivery vehicles must also be able to enter cells through the cell membrane, either by passive or active uptake. Important factors for cellular uptake of nanocarriers is the particle size and surface properties. Particles with the size of tens to hundreds of nanometers have been shown to enter cells more effectively than individual small molecules [20]. The surface charge of nanoparticles affects the transfection efficiency, since the cell membrane possess a negative charge. Nanocarriers with a positively charge surface generally enter cells easier. Although bare nucleic acids are highly negatively charged molecules that are difficult to pass through the membrane, DNA nanostructures have been showed to penetrate the negatively charged cell membrane. [3, 77] Usually transfection reagents, such as cationic lipids and polymers, are needed to enhance intracellular uptake of nucleic acids, although these reagents can be cytotoxic to living cells. One of the most used transfection reagent is lipid-based transfection agent Lipofectamine®. However, some DNA nanostructures have been showed to enter cultured cells without the help of any transfection reagent, for example a tetrahedral DNA nanostructure alone was capable of entering cultured mammalian cells [31, 78]. The cellular uptake of DNA nanocarriers is mainly studied by fluorescence-based assays, e.g., confocal microscopy and flow cytometry. However, fluorescent labels may in some cases affect the assembly or cellular interactions of DNA nanostructures. One alternative method for quantification of cellular uptake of DNA origamis is quantitative polymerase chain reaction (qPCR). qPCR is used to

amplify and quantify DNA molecules in solution, therefore it could also be employed to quantify the M13mp18 scaffold of DNA origamis in cell lysates. [79]

Furthermore, cellular uptake mechanisms of drug loading carriers affect the drug efficiency. It is still unclear by which mechanism DNA nanostructures penetrate into cells. Possible active cellular uptake mechanisms for nanocarriers include phagocytosis or other endocytosis pathways, especially receptor-mediated endocytosis [77]. In the endocytosis pathways, cell membranes transports particles into the cell by forming a vesicle around the particles. The transported cargoes must be also able to escape from these endosomes [74].

Although various DNA nanostructures, such as DNA cages [31], DNA pyramids [78] and DNA nanotubes [80], have been reported to enter cells, the efficient transfection of DNA constructs is still challenging. Therefore, new approaches are needed for enhancing the cellular uptake of DNA nanomaterials. One approach is to encapsulate nucleic acids with virus capsid proteins. Mikkilä *et al.* [34] utilized purified cowpea chlorotic mottle virus (CCMV) capsid proteins (CP) as coatings for rectangular DNA origami structures. These virus capsid proteins can bind on the origami surface through electrostatic interactions. The morphology of DNA origami-CP complexes changed from rolled-structures to open tiles while increasing the fraction of CP, as shown in Figure 15f. In the open tile structure the origamis were completely encapsulated. According to this study, the cell uptake of DNA origamis could be raised with increasing CP concentrations. This might support the assumption that the rigid and compact DNA structures enter cells more efficiently than the flexible ones [4]. In addition, DNA origami has been encapsulated with PEGylated lipid membranes (Figure 15g), which were effectively uptaken by immune cells [33]. Another approach to improve cellular uptake is to modify the surface properties of DNA origamis using DNA intercalators. The DNA intercalators are small molecules that can form noncovalent interactions between planar bases of double-stranded DNA. The DNA origamis modified with intercalators have been demonstrated to be uptaken by cells more easily than the unmodified origamis [81].

The performance of drugs can be improved by targeted drug delivery and controlled drug release systems. When drug loading nanocarriers are in the bloodstream, they must not interfere with the veins or the surrounding tissue but with the target cells. Therefore, drug delivery vehicles should identify specific receptors at target cells or contain a logic gate that triggers the drug release at a specific location. Releasing drugs in a controlled manner reduces the distribution volume of drugs *in vivo*, thus decreasing side effects. [20] One common method to identify target cells is to incorporate specific ligands, such as peptides, aptamers, antibodies or folic acids, into DNA nanostructures. These ligands bind to receptors found at target cells. Aptamers are short single-stranded DNA or RNA oligonucleotides that specifically bind to various molecular targets. They also exhibit significant therapeutic effects. Incorporation of aptamers into pyramidal DNA nanostructures showed an enhanced intracellular uptake and selectively inhibit the growth of cancer cells [78]. These DNA pyramids contained multiple overhangs to which targeting ligands, aptamers, could attach, as shown in Figure 14. Another specific ligand, folic acid, binds to folate receptors that are selective tumor markers located in many cancer cells. In

one study, folate molecules were incorporated into DNA nanostructures for targeted delivery of siRNA to tumor cells [25]. These folic acid-conjugated nanostructures showed the greatest targeting efficiency among various cancer-targeting ligands.

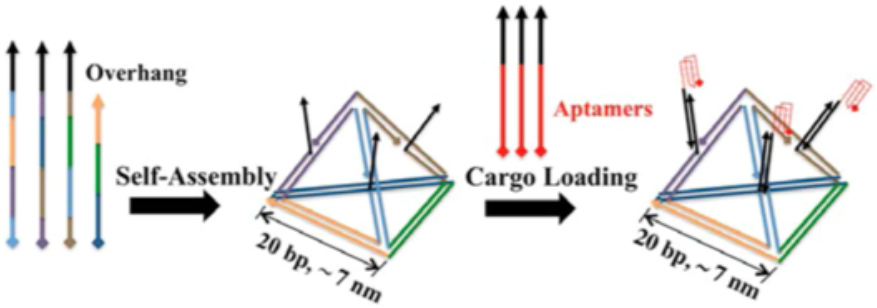

Figure 14: Aptamers used as targeting ligands. Three overhangs in the DNA pyramid allow attachment of aptamers to the nanostructure. [78]

DNA nanostructures are potential delivery vehicles for controlled drug release, since it is possible to design DNA nanostructures that can change conformation in response to sensing external signals in the environment [50, 82, 83]. One possible controlled drug release system is a box shaped DNA origami structure with a lid that can be opened to the response of specific oligonucleotide sequences used as 'keys' (Figure 15a) [50]. These DNA boxes could be used as nanocarriers with the potential to respond to particular biomolecular signals in cells. Another designed nanocarrier for controlled release of cargoes contained an aptamer-encoded logic gate (Figure 15e) [82]. The system could be locked using two similar aptamers or using two aptamers that are specific to two different targets. The gate opened only if the both aptamers recognized their targets simultaneously. Furthermore, a tweezer-like DNA nanostructure has been reported to be able to regulate its binding affinity with a protein in a distance-dependent manner [84]. This nanostructure could bind to the target protein when two ligands are located at an appropriate distance and that is referred to a closed state. However, the protein could be released in response to specific strand that increase the distance of the two ligands leading to an open state. This capture-release cycle could be repeated several times without changing the ligands and the target protein.

4.2 DNA origami and other DNA nanostructures as nanocarriers

Various hollow DNA origami constructs have been developed, as shown in Figure 15a. These hollow DNA constructs could be used to deliver cargoes into cells and protect cargoes from degradation in cellular environment. Ke *et al.* [85] designed a closed DNA tetrahedron with an inside cavity that could potentially used for encapsulating cargoes. Box-shaped DNA origamis have also been designed for the same intention [86, 50].

As discussed in the previous section, various DNA nanostructures are able to enter to cells. This has inspired researchers to develop DNA nanocarriers for delivering a wide range of molecules including doxorubicin, siRNA, CpG sequences and antibodies. One of the most used model molecules for cellular delivery are fluorescent dyes which can be used for confirming the cellular uptake of DNA delivery vehicles using fluorescent microscopes.

Doxorubicin (Dox) is a potent anticancer drug that can intercalate the DNA duplex and inhibit macromolecular biosynthesis. However, free Dox causes side effects and has poor selectivity. Zhao *et al.* [87] developed tubular DNA origami nanocarriers with different degrees of twist that enables regulating the release of Dox *in vitro* (Figure 15b). This delivery system was capable of entering breast cancer cells and inducing cell death. In another study, Jiang *et al.* [22] managed to deliver doxorubicin not only into regular human breast adenocarcinoma cancer (MCF 7) cells but also into Dox-resistant cancer cells using triangular- and tubular-shaped DNA origami structures shown in Figure 15b. The DNA origami nanocarrier enhanced cell death of resistant MCF7 cells. In addition, doxorubicin has been delivered into cells *in vivo* using triangle-shaped DNA origami nanocarriers [24]. This delivery system examined by fluorescence imaging showed enhanced tumor targeting and long-lasting tumor accumulation without observable systemic toxicity in nude mice in comparison to Dox alone. These presented DNA origami nanocarriers could serve as potential delivery systems for anticancer therapy. DNA origamis seem to possess various advantages as antitumor drug carriers compared with other DNA nanostructures such as wireframe cages. For example, DNA origamis could load more doxorubicin than the DNA nanocages. Furthermore, DNA origami can be designed in sizes ranging from ten to several hundred nanometers with controlled three-dimensional geometry, while the size of DNA cages can only vary between approximately 7–20 nm. [24]

Moreover, various DNA-based assemblies could be used for controlled and targeted release of Dox. For example, the cellular delivery of Dox for cancer therapy could be enhanced by multifunctional aptamer-based DNA nanoassembly [75], shown in Figure 15h. As discussed earlier, aptamers can be used to guide delivery vehicles to target cells. DNA-based multilayer nanofilms have also been reported to release Dox in a controlled way in serum conditions [83]. The nanofilms consisted of homopolymer as a template and three-dimensional DNA origami structures with Dox incorporated to it. The electrostatic interaction between the positively charged homopolymer and the negatively charged DNA was modulated by the change in pH conditions, which led to the release of some of the Dox-incorporated DNAs from the film. The release profile of Dox was dependent on the properties and shapes of the 3D DNA structures. The structure of the nanofilms can be seen in Figure 15h.

Apart from aptamers, DNA nanocarriers could also be loaded with various other functional nucleic acids, including antisense oligonucleotides, small interfering RNAs (siRNAs) and microRNA, that have high potential for diagnostic and therapeutic purposes [3]. siRNAs are chemically synthesized RNA sequences that can bind complementary mRNA molecules and inhibit them from synthesizing proteins. DNA nanostructures can be utilized for delivering siRNAs into cells in order to prevent

the expression of a certain gene that causes disease. Nanocarriers are also used to improve the cellular uptake and the stability of siRNA against enzymatic degradation. Kocabey *et al.* [88] investigated the ability of folate-modified DNA nanotubes loaded with siRNAs to silence a target gene. DNA nanotubes were capable to enter cells but they did not succeed in gene silencing. The structure of the DNA nanotube is shown in Figure 15c. However, Lee *et al.* [25] managed to create gene silencing system that used DNA tetrahedral nanostructures with folate and peptide targeting for siRNA delivery to tumor cells *in vitro*. Figure 15c shows the DNA tedrahedron structure with siRNA molecules hybridized to it and modified with tumor targeting ligands. The gene silencing efficiency was noticed to depend on the spatial orientation and the density of the ligands.

In addition to anticancer therapeutic and gene silencing delivery systems, DNA nanostructures could be utilized as potential immunotherapeutic carriers. When DNA nanocarriers are loaded with unmethylated cytosine-phosphate-guanosine (CpG) oligonucleotides, they can induce immune responses in order to protect body from harmful substances. CpG-DNA complexes could serve as therapeutic agents against a wide range of diseases such as cancer and allergic diseases. DNA nanostructures could be used to protect these CpG sequences from degradation and enhance both cellular uptake and specific targeting of CpG sequences. Schüller *et al.* [23] used a tubular DNA origami structure covered with tens of CpG sequences to induce immune responses in spleen cells (Figure 15d). These origami tubes showed greater immunostimulatory effects than the same amount of CpG sequences loaded to a standard transfection reagent (Lipofectamine) system. The DNA tubes did not show any detectable toxicity in contrast to Lipofactamine. In addition, Mohri *et al.* [89] designed a branched DNA structure using oligodeoxynucleotides containing CpG motifs (Figure 15d) that induced immune stimulatory activity in macrophage-like RAW264.7 cells. It was noticed that the more branched structure increased the cellular uptake and immune stimulatory activity but reduced the thermal stability. A DNA tetrahedron nanostructure has also been used as a nanocarrier for CpG and shown to efficiently enter RAW264.7 cells without the aid of transfection agents [21]. Furthermore, Sellner *et al.* [90] managed to induce immune response in muscle tissue of mice *in vivo* by using CpG-decorated DNA nanotubes. Importantly, neither plain DNA nanotubes nor CpG-sequences caused inflammatory effects in the muscle tissue, which was investigated by fluorescence and transillumination microscopy.

DNA nanostructures could also be loaded with a variety of peptides and proteins such as antibodies and enzymes. Such nanocarrier systems are highly desired, since functional proteins are not capable to enter cells easily due to their instability, large sizes and charged surfaces [5]. For example, DNA origamis have been loaded with antibody cargoes that induced growth arrest in leukemia cells (Figure 15e) [82]. Antibodies are molecules that recognize and neutralize antigens found in harmful agents. In addition, Yan *et al.* [91] used biotinylated DNA tetrahedral nanostructures to deliver CpG adjuvants and a model antigen streptavidin, which induced an antibody response *in vivo*. Adjuvants are molecules that can modify immune response to produce more antibodies against harmful substances. This antigen-adjuvant-DNA complex could be used as a delivery system for synthetic vaccines. Brodin *et al.* [5]

demonstrated a DNA-based carrier system for cellular delivery of functional enzymes. β-galactosidase enzyme served as a protein core and it was modified with a dense shell of oligonucleotides. This DNA-enzyme complex showed increased cellular uptake when compared with bare enzymes even using enzyme concentrations as low as 100 pM. DNA-functionalized enzymes retained also their catalytic activity after transfection.

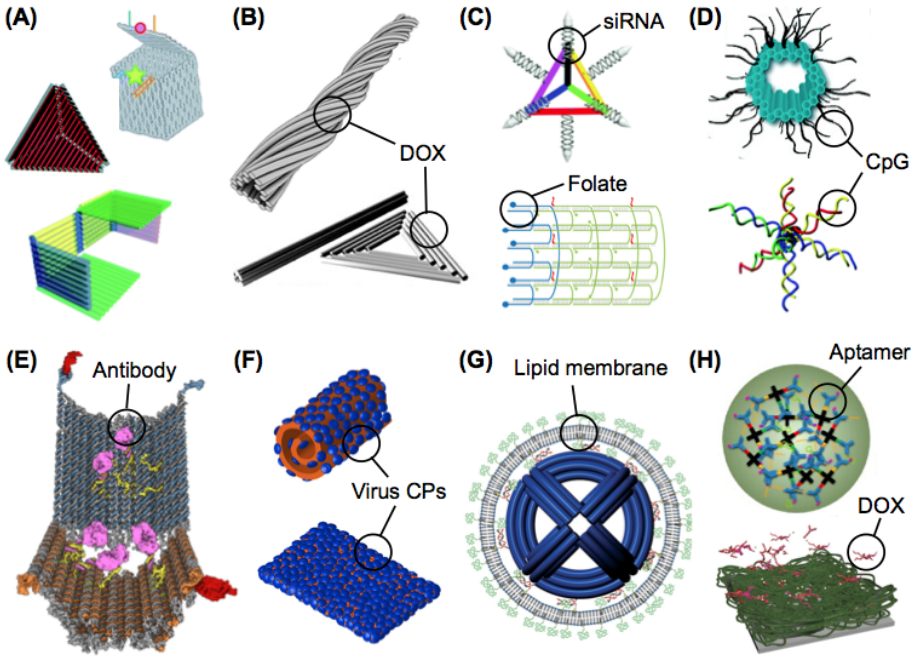

Figure 15: DNA-based delivery vehicles. (a) A DNA box for controlled release of cargoes [50] and hollow DNA origami constructs [85, 86] (b) Triangular- and tubular-shaped DNA nanocarriers for delivering Dox [87, 22] (c) A DNA tedrahedron [25] and tube [88] modified with folate targeting for delivering siRNA (d) A tubular DNA origami [23] and and a branched DNA structure [89] as delivery vehicles for CpG motifs (e) A DNA nanocarrier with an aptamer-encoded logic gate for controlled release of antibodies [82] (f) Virus-encapsulated DNA origamis as delivery vehicles [34] (g) A spherical DNA origami encapsulated with PEGylated lipid membranes [33] (h) An aptamer-based DNA nanoassembly for cellular delivery of Dox [75] and DNA-based multilayer nanofilm for controlled release of Dox in serum conditions [83]. Figure from Ref [4].

DNA nanostructures not only serve as potential carrier systems for cellular delivery but also they can act as molecular devices in living systems [4]. DNA templates can be used for directing protein assembly and functionalized DNA nanostructures could be used to recognize target proteins. DNA nanostructures could serve as scaffolds for precisely positioning proteins and they could be used to control enzymes that catalyze chemical reactions. As a result, several studies have demonstrated DNA-based nanoassemblies as enzyme cascade nanoreactors for controlling enzymatic reactions. Liu *et al.* [92] designed a tweezer-like DNA nanodevice to actuate the

activity of enzyme/cofactor pair. The enzyme and cofactor were placed at different arms of the tweezer, and the activation was regulated by changing the conformation between open and closed states as shown in Figure 16a. At a closed state the enzyme and cofactor were brought together for activation. Linko *et al.* [93] demonstrated GOx/HRP enzyme cascade reaction inside a DNA origami tube for detecting glucose. The tube was assembled from two distinct units with either glucose oxidase (GOx) or horseradish peroxidase (HRP) enzymes attached inside the origami unit, as can be seen in Figure 16b. They proposed that the tube could be used as a nanoscale diagnostic tool or for delivering enzymes into cells, that could be exploited, e.g., in enzyme replacement therapy.

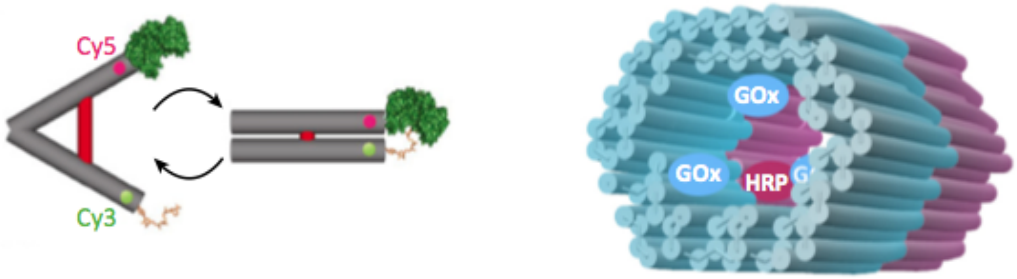

(a) (b)

Figure 16: DNA-based 'nanofactories' for controlling chemical reactions. (a) A tweezer-like DNA nanodevice for controlling enzymatic reactions. Fluorescence dyes Cy3/5 were used to characterize the open and closed states of the tweezer. [92] (b) The enzyme cascade reaction was demonstrated by attaching HRP and GOx enzymes inside the DNA origami tube [93].

4.3 Therapeutic applications

Enzyme replacement therapy (ERT) is a potential approach for treating some lysosomal storage diseases (LSDs), such as Gaucher disease and Fabry disease. ERT is currently approved for treating six LSDs [94]. LSD symptoms can greatly vary but typically they include central nervous system disorders. LSD results from the failure in the activity of lysosomal enzymes that transport waste materials and foreign substances into lysosomes, where they are degraded. If one of these enzymes is absent or presence in too small amounts, the recycling process will be disturbed causing the waste materials to accumulate within the lysosome and the cell. In enzyme replacement therapy, lysosomal enzymes can be delivered, e.g., by infusion into the systemic circulation, to diseased cells where they move to lysosomes. ERT is shown to treat LSD in certain organs and tissues but the delivery of enzymes into tissue of central nervous system remains challenging. Therefore, efficient delivery systems, that are able to transport enzymes to all the organs diseased by LSDs, need to be developed. [95] DNA nanostructures could serve as potential delivery nanocarriers for controlled circulation, organ targeting, cell entry and release of lysosomal enzymes.

A few studies have demonstrated DNA nanostructures as potential delivery vehicles for enzymes [5, 93].

Prodrugs refer to a biologically inactive derivates of drug molecules that must undergo enzymatic or chemical transformation *in vivo* to release the active drug. Prodrugs are designed to enhance pharmacological properties of drugs, such as permeability, aqueous solubility, chemical stability and bioavailability that is defined as a degree and rate at which a drug becomes available at a target organ. In addition, prodrugs have been used to improve the transport and selectivity of drugs to their intended target. There are two main classes of prodrugs: carrier-linked prodrugs and bioprecursor prodrugs. The carrier-linked prodrug is composed of a carrier to which drugs are covalently linked. The carrier system undergoes transformation and release the carrier and the drug once they are delivered to the target place. Bioprecursor prodrugs do not contain a carrier but they are transformed metabolically or chemically into an active drug. [96] The selectivity of drugs to their intended targets might be possibly attained by using DNA nanostructures as a part of carrier-linked prodrug. DNA nanocarriers can be modified to undergo transformations in response to specific signals causing the release of cargoes [50, 82], which were already discussed in Chapter 4.1.

Furthermore, as mentioned earlier DNA nanostructures could serve as potential nanocarrier systems for anticancer therapy. Anticancer drugs are used in chemotherapy to destroy cancer cells. However, these chemotherapeutic drugs have poor selectivity and therefore they affect both cancer cells and normal cells causing side effects. The drug selectivity to cancer cells can be enhanced by loading them to nanocarriers that have shown a more efficient passive tumor-targeting and an accumulation in tumor tissue in comparison to bare anticancer drugs. This phenomenon is known as enhanced permeability and retention (ERP) effect. Nanocarriers could be also utilized to encapsulate and deliver poorly soluble anticancer drugs. [97] Moreover, another approach to improve selectivity is to use prodrug technology in which anticancer prodrugs could be designed to target specific molecules located in high concentrations in tumor cells [96]. There are only a few clinically approved anticancer drug delivery systems that are based on liposome, polymer and protein carriers [97, 98]. Various other delivery systems are under development. Several studies have demonstrated that DNA nanostructures could be used to deliver anticancer therapeutic agents such as doxorubicin, CpG motifs and antibodies into cells, see Chapter 4.1. The delivery of CpG motifs could serve as immunotherapy for cancer cells. Moreover, these nanostructures could be modified to selectively bind to cancer cells, for example aptamers incorporated in DNA nanostructures can be utilized to target specific cancer cells [75]. In addition, DNA origamis are found to exhibit ERP effect [24].

4.4 Challenges with DNA nanocarriers

Several challenges must be overcome and various aspects must be studied in more detail before DNA structures could be used as delivery vehicles in clinical applications. The properties of DNA nanostructures need to be further studied *in vitro* and *in vivo*

in order to fully understand their behavior in living organisms. Another important aspect to study is the transportation mechanism of DNA nanomaterials into cells including their intracellular route and fate and also their pharmacokinetic properties, i.e., in vivo circulation and distribution. Attention must also be focused on the selective uptake of DNA nanocarriers by target cells. DNA constructs are shown to remain stable in cell lysates and culture media at least a day. However, further research is needed to examine the effect of the structure of DNA constructs on its stability [99]. In order to improve the circulation time of DNA nanocarriers, they can be coated for example with virus capsids [34] or lipid bilayers [33]. It is also important to study how the physical and chemical properties of DNA nanostructures affect their intracellular behavior. [3, 99]

In addition to these biologically related problems, the high cost and ineffective production methods of DNA nanostructures limits their use in practical biomedical applications. The fabrication of 1 g of megadalton-sized DNA origami objects costs approximately 100,000 dollars [4], while 1 g of polymer materials used as drug delivery systems can cost less than 1 dollar [99]. The high cost is partly due to the lack of an efficient purification method for preparing DNA-based asseblies with high concentrations. New methods are needed for purification and scaling up the fabrication of DNA origamis in order to reduce the production costs. The field of DNA nanotechnology is constantly growing and developing. Therefore, it is expected that the production costs for 1 g of DNA origami will fall to 1,000 dollars in the next few years if more efficient purification methods and printing techniques for sequence synthesizing are developed. [4, 100] One approach to solve the purification problem is to use PEG purification that is based on adding PEG polymers as a precipitating agent to DNA solutions. The method has shown to efficiently purify various DNA origami structures from excess staples with high yields. [101] Recently, the development of high-cell-density bioreactors increased the production of ssDNA for scaffolded DNA origamis from the micro and milligram scale to the gram scale per one liter reaction volume [102].

Furthermore, the size of DNA origamis should be extended in order to increase the amount of payloads [3]. One approach for scaling up the size of DNA origamis includes forming a DNA origami from multiple origami structures, as discussed in Chapter 3. Moreover, the traditional scaffold strand from bacteriophage M13mp18 could be replaced by other scaffold strands, for example longer scaffold strands can be prepared by using polymerase chain reaction (PCR) amplification [103]. Although the self-assembly of DNA origamis generally results in correct assemblies, larger and more complex structures can lead to increasing assembly errors with lower yields. Therefore, it is important to understand the kinetics and thermodynamics of self-assembly between the components of DNA constructs. [20, 100]

5 Materials and methods

In this thesis, a DNA origami was used as a nanocarrier for the transfection of Streptavidin-Lucia luciferase (LUC) enzymes into human embryonic kidney cells (HEK293 cells) *in vitro*. The designed DNA origami is a hollow hexagonal tube with a molecular mass of about 4.5 MDa. The tube contains three biotin-linkers, which enables three LUC-enzymes to attach to it by the biotin-streptavidin interaction. Streptavidin-Lucia luciferase is a small enzyme with a molecular mass of 37 kDa. Luciferases are used in bioluminescence applications, for example Steptavidin-Lucia enzyme is utilized to detect streptavidin-biotin interactions. This work utilizes the bioluminescence phenomenon for detection of the activity of the delivered luciferase enzymes in cell lysates. The detected light is emitted from the reaction between luciferase enzyme and its coelenterazine based substrate. Figure 17 summarizes the main aim of this work. In addition, these DNA origami nanocarriers were coated with three different polymers to study the effect of the coatings on the activity of the LUC-enzymes attached to the origamis.

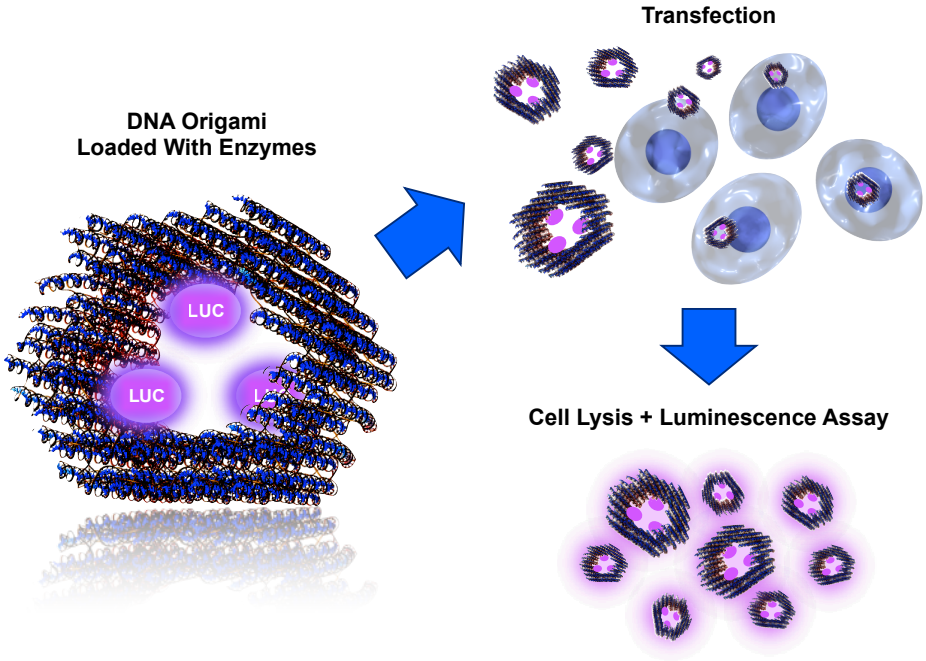

Figure 17: A DNA origami nanocarrier is loaded with three bioluminescence LUC-enzymes and transfected into cells *in vitro*. After transfection the cells are lysed and the activity of transported enzymes is measured from the cell lysates using coelenterazine-based bioluminescence assay. [104]

5.1 Preparation of LUC-origami complexes

The structure of the DNA origami, shown in Figure 18, was designed by Linko *et al.* [93, 105]. The designed hollow hexagonal tube (HT) has a length of about 30 nm and a width of about 27–33 nm. The wall thickness is 6–7 nm and the cavity is 14–21 nm wide. The tube contains three biotinylated strands (HTB) for the attachment of the streptavidin functionalized LUC-enzymes (STV).

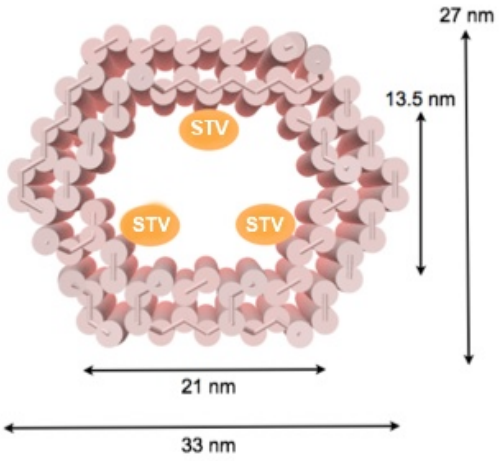

Figure 18: The dimensions of a DNA origami unit used as a nanocarrier. The inner surface of the origami contains three biotinylated strands for the functionalization of the origami. STVs indicate the positions to which streptavidin functionalized LUC-enzymes can attach. Adapted from [93].

The DNA origamis were prepared by folding a 7249 bases long single-stranded DNA scaffold from virus M13mp18 (from Tilibit nanosystems or New England Biolabs) with a set of short staple strands purchased from Integrated DNA Technologies. As mentioned above, three of the staple strands contained biotinylated binding sides for streptavidin functionalization. Moreover, the origamis were labeled with fluorescent Cy3 tags for transfection studies. The origami contained 5 binding sites for the fluorescent tags. The overhangs of the binding site strands are complementary to the Cy3-modified strand, thus enabling a desired attachment. All the staple strands included in the DNA origami structure are presented in Appendix A. The M13mp18 scaffold strand and the staple strands were mixed with a folding buffer containing 10x TAE buffer Ultrapure (400 mM tris(hydroxymethyl)aminomethane (Tris), 10 mM ethylenediaminetetra acetic acid (EDTA) and glacial acetic acid for adjusting the pH to 8.3, from USB Corporation), magnesium chloride ($MgCl_2$) and sodium chloride (NaCl). The concentrations of the components needed for folding DNA origamis are shown in Table 2. The staple strands were added in 10-fold excess concentration to the scaffold.

The origami solution with the total volume of 100 µl was annealed using G-Storm G1 Thermal Cycler. The origamis were first heated to 65 °C and then cooled down

to 60 °C by 1.0 °C decrease in 15 minutes. From 60 °C the origamis were cooled down to 45 °C by 0.25 °C decrease in 45 minutes after which they were stored at 12 °C inside the thermal cycler before the program was stopped. After folding, the structures were stored at 4 °C in the refrigerator.

Table 2: The volumes and concentrations of the components for preparing DNA origami nanocarriers. Final concentrations signify the concentrations in the origami reaction solution.

Component	**Volume**	**Concentration**	**Final Concentration**
M13mp18 scaffold	20 µl	100 nM	20 nM
Staples	40 µl	500 nM	200 nM
Folding buffer:			
TAE buffer	10 µl	10x	1x
NaCl	10 µl	50 mM	5 mM
$MgCl_2$	20 µl	100 mM	20 mM

The excess amount of staples was removed in a non-destructive spin-filtering process using Eppendorf Centrifuge 5424R. The spin-filtering process was performed using Millipore Amicon Ultra 0.5 ml Centrifugal Filters with 100 kDa molecular weight cut-off. 50 µl of DNA solution was mixed with 450 µl of filtration buffer (5 mM NaCl, 20 mM $MgCl_2$, 1x TAE, pH 8.57) and injected into the filter. The solution was spun with 14,000 rcf (relative centrifugal force) for 3 minutes at 20 °C. Then flowthrough was discarded and 450 µl of fresh filtration buffer was added to the filter. The sample was spun in total 4 times repeating the procedure above, expect for the last round the buffer was changed to HEPES-NaOH (6.5 mM HEPES, pH 6.8) and the centrifugation time was set to 5 minutes. After the last spinning, the solution was collected from the filter with a pipette and the filter was turned upside down in a fresh container and spun 2 minutes at 1,000 rcf to collect the rest of the solution. After filtration the volume of the solution was typically brought from 500 µl down to 17–24 µl. The theoretical concentration of the origamis before filtering is 20 nM and after filtering about 40–60 nM if the yield is 100 %.

Streptavidin-Lucia luciferase (LUC) enzyme (100 µg/ml stock solution, from InvivoGen) was added to origamis in 10–20-fold excess concentration. The solution was incubated at least 6 h or overnight at room temperature. The excess amount of added LUC-enzymes was removed by the same filtering method as above. After filtering the origamis were stored at 4 °C. In order to ensure that the filtering procedure functions efficiently for the LUC-enzymes, the bioluminescence assay was performed for filtered and unfiltered LUC-enzymes, see Appendix B.

In addition, to be sure that the LUC-enzymes function properly, the bioluminescence assay was performed for the free LUC-enzymes. The bioluminescence intensity of Streptavidin-Lucia enzyme was measured as a function of time by mixing 10 µl of pure LUC-enzyme (100 µg/ml) with ready 50 µl of coelenterazine-based luminescence

assay reagent (QUANTI-Luc, InvivoGen). As a blank, 10 µl of autoclaved water was used and mixed with the reagent. The bioluminescence was immediately detected after the mixing by using a luminometer (BioTek Cytation 3). The first data points were recorded 10 seconds after adding the reagent. The same luminometer is used in all bioluminescence measurements in this thesis. The luminescence decay shown in Figure 19 demonstrates that the reaction is very fast. Therefore, in each measurement only the luminescence decay is monitored. The luminescence decay corresponded to the typical signal produced by coelenterazine-based substrate (InvivoGen).

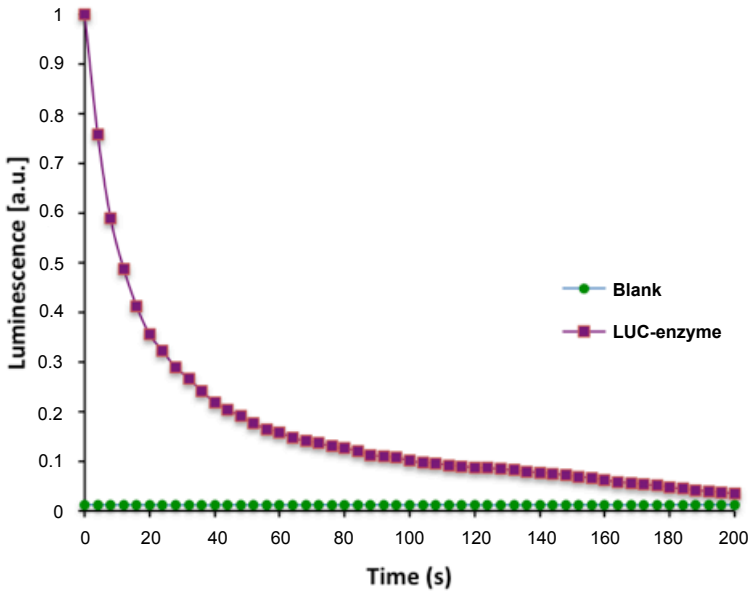

Figure 19: The luminescence intensity of the free LUC-enzymes (violet) as a function of time. Autoclaved water was used as a blank (green). The maximum intensity of the free LUC-enzymes was normalized to 1.

5.2 Analyzing DNA origamis

The concentrations of the DNA origamis were determined using BioTek Eon Microplate UV/VIS Spectrophotometer. DNA origami concentrations (c_{DNA}) were estimated using Beer-Lambert relation,

$$A_{260} = \varepsilon_{260} c_{DNA} l, \tag{1}$$

where A_{260} is the absorbance at 260 nm wavelength, ε_{260} is the approximated extinction coefficient ($0.9 * 10^8$ M^{-1} cm^{-1} [67]) and l is the length of the light path in centimeters (0.05 cm).

The quality of folding and purification of the DNA origami units were verified by agarose gel electrophoresis using BIO-RAD Power Pac Basic equipment. Agarose gel electrophoresis is a widely used method for separating DNA by size. In electrophoresis, an applied electrical field moves the negatively charged DNA toward a positive

electrode through an agarose gel matrix. 2 % agarose gel was prepared by dissolving 2 g of agarose (from Sigma-Aldrich) into 100 ml of 1 x TAE buffer containing 11 mM Mg^{2+}. The solution was stained with 80 µl of ethidium bromide (EthBr) solution (0.625 mg/l). The binding of EthBr to DNA intensifies the fluorescent signal of EthBr and thus enables the visualization of DNA under ultraviolet (UV) light. 1x TAE + 11 mM Mg^{2+} was used as a running buffer. Samples with the volume of 10 µl were stained with 2 µl of loading dye (6 X Blue Loading Dye from New England Biolabs). Since the spin-filtering process removes almost all the Mg^{2+} ions from the DNA origami solution [106], Mg^{2+} concentration of the filtered samples was increased to the same value as in the folding conditions that is about 20 mM. 10 µl of the sample solution was pipetted into the agarose gel wells. An M13mp18 scaffold strand was used as a reference sample containing 4 µl of M13mp18 scaffold strand, 6 µl of filtration buffer and 2 µl of loading dye. The gels were run with a constant voltage of 90 V for 45 minutes. The gel was visualized by ultraviolet light using BIO-RAD Gel Doc^{TM} EZ Imager.

The origamis were also imaged by TEM to verify the correct folding. TEM images were taken with Tecnai 12 Bio Twin instrument. The samples were prepared on Formvar carbon coated copper grids (Electron Microscopy Sciences). A 3 µl drop of the sample solution was placed on the grid and blotted away with a piece of filter paper. The samples were negatively stained twice with 0.5 % uranyl acetate in Milli-Q water.

5.3 Preparation of LUC-origami-polymer complexes

The origami-enzyme complexes (LUC-origamis) and free luciferase enzymes were coated with varying amounts of three different cationic block-copolymers to control enzyme reaction rates in a bioluminescence assay. The used polymer coatings included poly(2-dimethylamino)ethyl methacrylate (PDMAEMA) homopolymer (HP) and two different block-copolymer structures PDMAEMA-PEG (AB-type) diblock copolymer and PDMAEMA-PEG-PDMAEMA (ABA-type) triblock copolymer. These cationic polymers bind electrostatically to negatively charged DNA origamis. The structural formulas of the polymers are presented in Figure 20. Further information about the synthesis and properties of these polymers can be found in the reference [107]. Kiviaho *et al.* [107] explored the electrostatic binding between these polymers and a brick-like DNA origami. The biocompatibility of these polymers was also investigated. The biocompatibility of PDMAEMA could be enhanced by incorporating poly(ethylene glycol) (PEG) into the PDMAEMA. Cationic polymers, such as PDMAEMA, could be possible used to improve the cell transfection of DNA origamis.

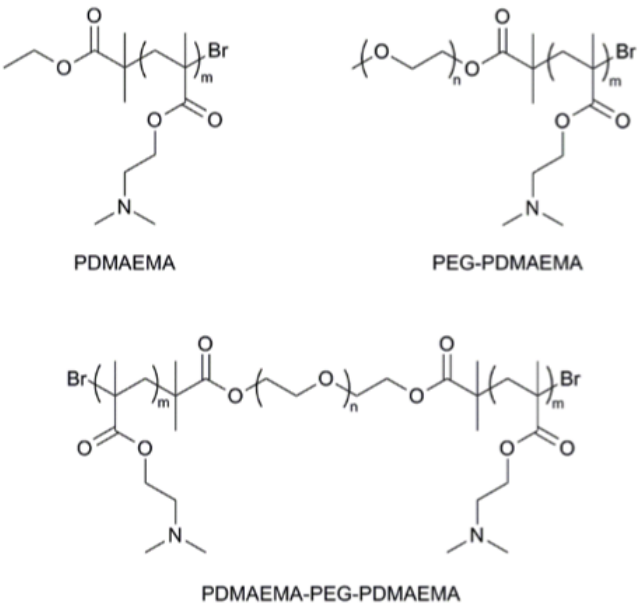

Figure 20: The structural formulas of homopolymer PDMAEMA, diblock copolymer PDMAEMA-PEG and triblock copolymer PDMAEMA-PEG-PDMAEMA. [107]

In this experiment, the LUC-origamis were filtered by the same method as mentioned earlier but HEPES-NaOH (6.5 mM HEPES, pH 6.8) was used as a filtration buffer in all rounds. The polymers dissolved in the HEPES/NaOH buffer were added in 10×, 100× and 1000× excess amounts to the LUC-origamis and mixed with the buffer so that the final concentration of the origamis in each sample was 35 nM. A LUC-origami sample without polymer coating was also prepared with the same concentration. A control assay was prepared by titrating free LUC-enzymes, which were diluted with HEPES-NaOH buffer, to correspond the behavior of LUC-origami samples without added polymers (similar decay kinetics and parameters in bioluminescence assay). The free LUC-enzymes were treated with polymers exactly the same method as the LUC-origami samples. The samples were incubated for 2 h. After the incubation, the activity of the enzymes was analyzed by the bioluminescence assay described in Chapter 6.1.

5.4 Cell culture and treatment with LUC-origami complexes

Cell transfection was performed for the fully characterized and tested LUC-origami, bare origami and free LUC-enzyme samples. In addition, the components of the DNA origami, including short DNA strands, i.e. staples and a long scaffold strand, were used as controls. The samples were transfected into human embryonic kidney cells (HEK293 cells) from ATCC. HEK cells were maintained in growth media containing Dulbecco's modified Eagle's medium (DMEM) with high glucose (4.5 g/l), L-glutamine (4.0 mM), sodium pyruvate (4.0 mM), glutamine and penicillin streptomycin mix (from HyClone-Thermo Scientific), supplemented with 10 % (v/v)

fetal bovine serum (FBS) (from Gibco-Life Technologies). Cells were maintained at 37 °C in a humidified (5 % CO_2) incubator.

1 µg of each sample was transfected into HEK cells transiently with or without a transfection reagent polyethylenimine (PEI) (25 kDa, linear, from Polysciences # 23966-2). PEI is a cationic polymer that attaches to DNA and turns it into positively charged particles that bind to anionic cell surfaces. The concentrations of transfected LUC-origami and bare origami were approximately 1 nM. The concentration of the free luciferase sample (LUC (adjusted)) was titrated to match the luminescence decay curve of LUC-origami sample shown in Chapter 6.2.1. The cells were then let grow at 37 °C for 12-36 h to allow the DNA origami transfection. After the transfection, the cells were fixed in 4 % paraformaldehyde (PFA) and washed three times with phosphate-buffered saline (PBS) in order to remove all the added origamis and other molecules that are left on the surface of the cells or the cell culturing plates. Cells were lysed using coelenterazine-based substrate 12 h after the transfection and the bioluminescence assay was immediately performed.

In addition, the DNA origamis were labeled with fluorescent Cy3 dyes in order to detect the transfection by confocal microscopy. The HEK293 cell nuclei was labeled with DAPI (Sigma Aldrich) nucleic acid stain. Fluorescent labeling enables the detection of target molecules, since fluorescent molecules respond distinctly to light compared to other molecules. In confocal microscopy, images are taken from different focal planes through samples and then combined to form a stack. Confocal microscopy images were taken with Leica TCS SP8 microscopy (405 nm violet blue diode laser and 514 nm argon blue laser) using a 63X objective (HC PL APO CS2 with glycerol).

6 Results and discussion

This section is divided into two subsections in order to distinguish the activity measurements of the LUC-origami-polymer complexes from the methods to verify the delivery of LUC-enzymes into the cells. But first, the results from the characterization of the LUC-origami complexes are presented.

The DNA origami nanocarriers were characterized by transmission electron microscope and agarose gel electrophoresis, as shown in Figure 21. The designed model of origamis corresponded the structure of folded DNA origamis as can be seen from TEM images. Moreover, agarose gel electrophoresis confirmed the efficient purification of the origamis from the excess staple strands. In agarose gel electrophoresis figure, the left sample named S signifies M13mp18 scaffold strand that was used as a reference. Folded HTB signifies DNA origamis right after folding, and filtered HTB signifies filtered DNA origamis. The excess staple strands in the folded HTB sample correspond the lowest bright band in the folded HTB column. Because of the small size of staple strands, they move faster in the gel than the origami itself. HTB origamis loaded with luciferase enzymes (LUC+HTB) were also analyzed by gel electrophoresis. The binding of the LUC-enzymes greatly affected the running speed of the origami. LUC-enzymes seem to bind efficiently and also nonspecifically to origamis, since the origami band totally disappeared in the gel. Due to the nonspecific binding of Streptavidin-Lucia enzymes with an isoelectric point (pl) of 5.8, the charge of the LUC+HTB sample may be highly negative in the filtration buffer (pH 8.57). This may cause the origamis to shift faster towards the positive side of the gel.

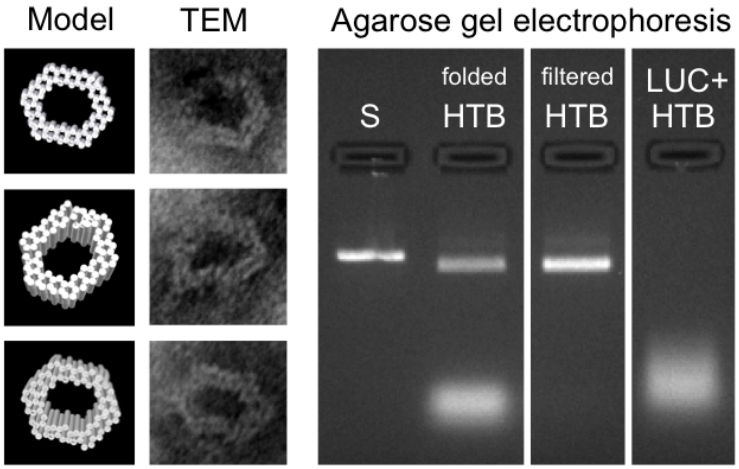

Figure 21: The designed model and TEM images of the DNA origami. Agarose gel electrophoresis of the DNA origamis (folded and filtered HTB) and the origamis loaded with LUC-enzymes (LUC+HTB). Agarose gel electrophoresis showed efficient purification of origamis (HTB) from excess staple strands that correspond the lowest bright band in the folded HTB column. A M13mp18 scaffold strand was used as a reference (S). [104]

As the enzymes were found to bind to DNA origamis also nonspecifically, the

real enzyme concentration is much more than three times the origami concentration. The origami tube contained three binding sites for LUC-enzyme. Because of the nonspecific binding, the real enzyme concentration in origami samples was hard to control and measure. In the following experiments, the free enzyme concentration was titrated to match the behavior of the origami sample with enzymes attached (LUC-origami).

6.1 The activity measurements of LUC-origami-polymer complexes

The polymer coated LUC-origamis were analyzed by the bioluminescence assay to study the effect of the coatings on the enzyme activity. The used polymer coatings included homopolymer (HP) PDMAEMA, diblock copolymer (AB) PDMAEMA-PEG and triblock copolymer (ABA) PDMAEMA-PEG-PDMAEMA in 10×, 100× and 1000× excess concentrations with respect to DNA origami. The bioluminescence assay was measured as a function of time by mixing 10 µl of polymer coated LUC-origamis with ready 50 µl of coelenterazine-based luminescence assay reagent. The bare LUC-origami sample that did not contain polymers was also analyzed, and as a blank 10 µl of HEPES/NaOH buffer (pH 6.8) was used. The reagent was mixed with all of the samples at the same time, and the measurement started 10 seconds after adding the assay reagent to the origami solutions. The control assay, only enzymes and polymers, was performed exactly at the same method. The luminescence decay for the samples obeys a standard stretched exponential behaviour [108]

$$I(t) = A \exp[-(t/T)^{\beta}], \tag{2}$$

where I = luminescence intensity, A = constant, T = time constant of the reaction and β = stretching exponent ($0 < \beta \leq 1$). The luminescence assays were analyzed using the above-mentioned equation (2). The example of the normalized decay assay ($A = 1$) and the fits for the HP coated LUC-origamis can be seen in Figure 22A. Time constants from the fits for all the origami-polymer complexes (HP, AB and ABA-coated) are shown in Figures 22B, 22C and 22D. The fitting parameters A and T for all the samples are presented in Table 3. The curves were fitted to data points using MATLAB.

LUC-enzymes showed appropriate catalytic activity in all samples indicating that the added polymer is not capable of blocking the enzyme activity completely. All the samples showed stretched behavior in the decay kinetics (β is 0.7-0.9). The polymer coatings seem to change the enzyme activity for LUC-origami, in other words they seem to affect the reaction rates of the enzymes in the origami samples. Instead, the polymer coated LUC-enzymes did not show any change in their behavior when increasing the amount of polymers. As can be seen from Table 3, the characteristic reaction time constant (T) was gradually prolonged for LUC-origamis but not for the free enzymes when the amount of polymers was increased. The prolongation was the most significant for the LUC-origami coated with homopolymer and with AB-type block-copolymer in 1000× excess amount, as these thickest coatings resulted

in about 2 times greater T value compared with the bare LUC-origamis (no polymer). The change in T value for AB-type polymer was not as significant as it was for homopolymer. T values for ABA-type polymer remained almost the same in all polymer concentrations. The results indicate that the observed prolongation resulted from the attachment of LUC-enzymes to origamis. One explanation for this might be that the polymer coating of the origami limits the accessibility of the enzymes and restricts the diffusion rate of the substrate [107].

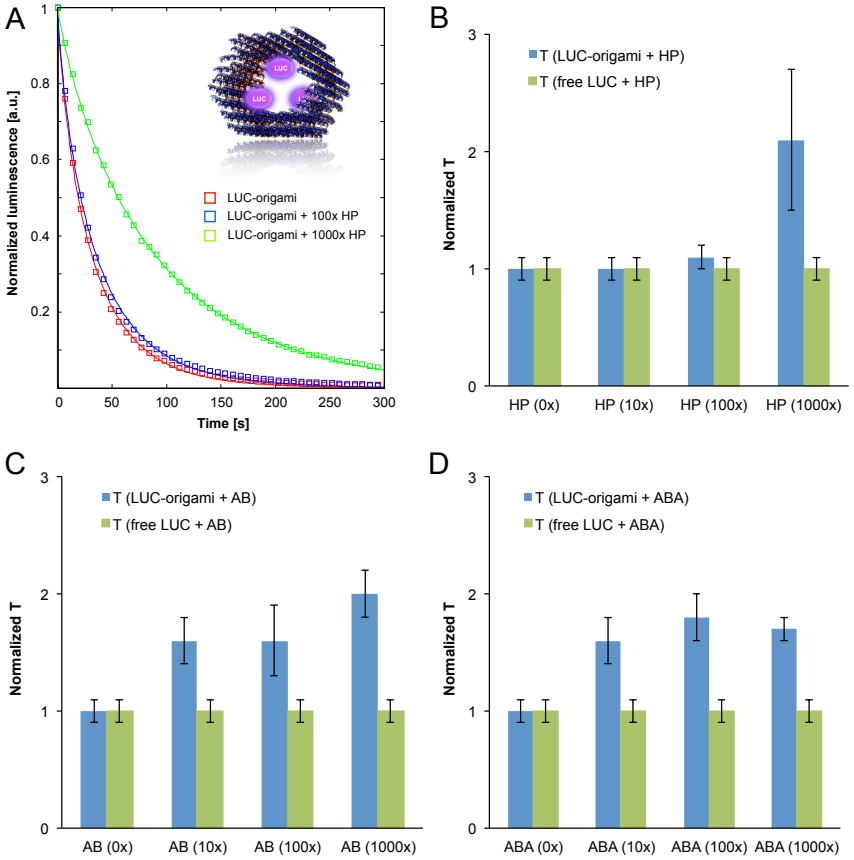

Figure 22: A) Normalized luminescence decay data points and fitted curves for bare LUC-origami sample (red) and for LUC-origami coated with PDMAEMA homopolymer (HP) 100× (blue) and 1000× (green) excess amounts. 10× excess amount of HP was omitted for clarity because it follows the same decay as that of LUC-origami + 100× HP. The curves were fitted using the stretched exponential equation (2). B)-D) Fitted normalized time constants of the luminescence decay for LUC-origami (blue) and free LUC enzymes (control assay without origamis, green) complexed with HP, AB and ABA, respectively. Time constants were determined with four different polymer concentrations (0×, 10×, 100× and 1000× with respect to DNA origami). Each case without added polymer has been normalized to 1. [107]

Table 3: Fitted normalized time constants T and the stretching exponents β for all the LUC-origami and free LUC samples used in the bioluminescence assay. The similar amount of enzyme is added to each sample.

Polymer (amount/ DNA origami)	**LUC-origami**	**Free LUC**
No polymer	$T = 1 \pm 0.1$ (normalized) $\beta = 0.81 \pm 0.02$	$T = 1 \pm 0.1$ (normalized) $\beta = 0.85 \pm 0.07$
HP (10x)	$T = 1.0 \pm 0.1$, $\beta = 0.84 \pm 0.03$	$T = 1.0 \pm 0.1$, $\beta = 0.85 \pm 0.05$
HP (100x)	$T = 1.1 \pm 0.1$, $\beta = 0.83 \pm 0.03$	$T = 1.0 \pm 0.1$, $\beta = 0.85 \pm 0.05$
HP (1000x)	$T = 2.1 \pm 0.6$, $\beta = 0.87 \pm 0.03$	$T = 1.0 \pm 0.1$, $\beta = 0.85 \pm 0.05$
AB (10x)	$T = 1.6 \pm 0.2$, $\beta = 0.85 \pm 0.03$	$T = 1.0 \pm 0.1$, $\beta = 0.85 \pm 0.05$
AB (100x)	$T = 1.6 \pm 0.3$, $\beta = 0.76 \pm 0.07$	$T = 1.0 \pm 0.1$, $\beta = 0.85 \pm 0.05$
AB (1000x)	$T = 2.0 \pm 0.2$, $\beta = 0.80 \pm 0.07$	$T = 1.0 \pm 0.1$, $\beta = 0.85 \pm 0.05$
ABA (10x)	$T = 1.6 \pm 0.2$, $\beta = 0.73 \pm 0.04$	$T = 1.0 \pm 0.1$, $\beta = 0.85 \pm 0.05$
ABA (100x)	$T = 1.8 \pm 0.2$, $\beta = 0.79 \pm 0.03$	$T = 1.0 \pm 0.1$, $\beta = 0.85 \pm 0.05$
ABA (1000x)	$T = 1.7 \pm 0.1$, $\beta = 0.81 \pm 0.07$	$T = 1.0 \pm 0.1$, $\beta = 0.85 \pm 0.05$

6.2 Determination of the delivery of LUC-origami complexes into cells

After the characterization of LUC-origami complexes, the bioluminescence assay was performed to verify the proper enzyme activity in the LUC-origami sample. After this, the LUC-origamis were transfected into the cells, and the transfection was then examined by confocal microscopy and bioluminescence assay.

6.2.1 Cell-free bioluminescence assay

The bioluminescence intensity for the spin-filtered LUC-origami (LUC+HTB), free LUC-enzyme and bare origami (HTB) were analyzed. The bioluminescence intensity of the samples was measured similarly as explained in previous sections. The luminescence decay curves and the relative luminescence intensities of the samples

are shown in Figure 23. The concentration of the free enzyme sample was titrated to match the luminescence decay curve of the LUC+HTB sample. Typically the concentration of adjusted free luciferase was 500–800 nM, i.e. 8–20 times the origami concentration (35–100 nM). LUC-origami samples might have contained a modest amount of enzymes that were not removed in the spin-filtering process, see Appendix B. In addition, it seems that all the added enzymes remained nonspecifically bound to origamis after purification. The concentrations of LUC-origami samples were calculated using the equation (1). The luminescence decay for the LUC-origami and the free LUC-enzyme corresponded the typical decay for the luciferase enzyme (100 µg/ml) shown in Figure 19. The bare origami did not show any activity.

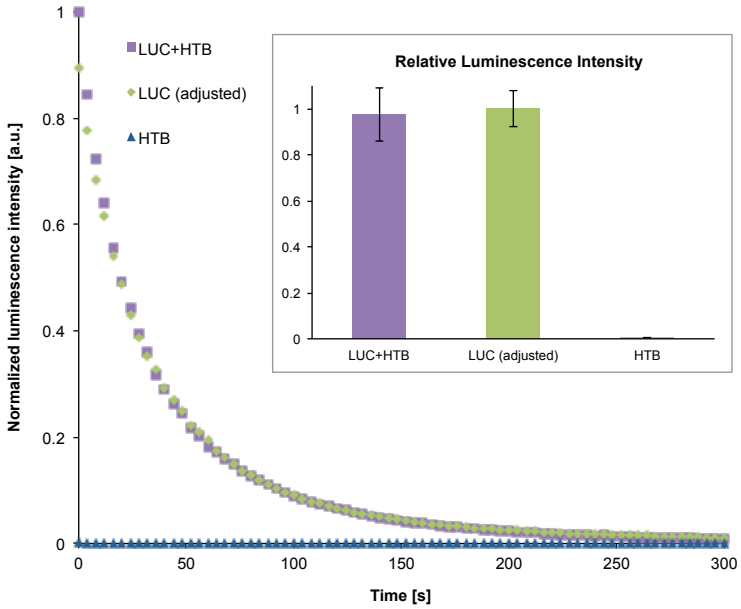

Figure 23: The luminescence decay for the LUC-origamis (LUC+HTB), the free enzymes (LUC adjusted) and the bare origamis (HTB) as a function of time. The maximum luminescence intensity for the LUC+HTB (violet) sample was normalized to 1 and it was compared to the maximum intensity of the LUC (green) and HTB (blue) samples. The mean values were calculated from three different measurements. [104]

6.2.2 Confocal microscopy

After the transfection experiments described in Chapter 5.4, the confocal microscopy images were taken to verify the proper transfection of DNA origamis. After 36 h of transfection, it seems that the origamis were co-localized with the cell nuclei as can be seen in Figure 24a-c. Cy3-labeled DNA origamis (red) overlay DAPI-labeled HEK293 cell nuclei (blue) as shown in Figure 24c. This suggests that the origami was successfully transfected into the cells. On the other hand, it might be possible that some of the origamis were only attached on the surface of the cell membrane.

In addition, the degradation of origamis in cell culture media was not studied in this thesis, and thus it might be possible that only the components of the origami were entered into the cells. In order to examine the transfection further, the activity of the delivered LUC was measured in the cell lysates using bioluminescence assay.

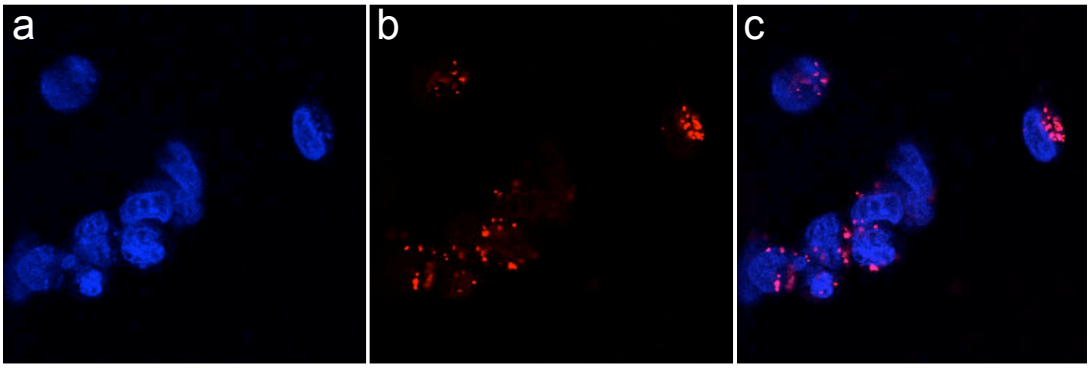

Figure 24: (a)-(c) Confocal microscopy images of DNA origami transfection. (a) DAPI-labeled HEK293 cell nuclei. (b) Cy3-labeled DNA origamis. (c) Overlay of the figures (a) and (b). [104]

6.2.3 Bioluminescence assay from cell lysates

The enzyme activity was detected from cell lysates after 12 h of transfection using the bioluminescence assay similarly as explained in Chapter 6.2.1. The luminescence decay for each sample was significantly slower when measured from cell lysates than from the HEPES/NaOH buffer (cell-free luminescence assay). In addition, the luminescence level of the transfected samples stayed the same over 10–15 minutes. This was mainly due to the dilution of the samples during the transfection experiments. Moreover, the luminescence intensity might have been affected by cellular compartments.

Figure 25 shows the normalized maximum luminescence intensities for all the samples transfected with or without PEI. Duplicate or triplicate samples was used to determine each measurement point in every measurement. Two left-side histograms show the luminescence intensity of transfected unfiltered LUC-origami (LUC+HTB), LUC+staples, LUC+scaffold and free LUC samples. The HTB was spin-filtered after folding, but not after the LUC has been added. Exactly the same amount of LUC was added to each sample. The LUC+HTB sample showed greatest luminescence intensity and the free LUC sample the slowest when the PEI was used as a transfection reagent. The luminescence intensity was slightly increased for the staples+LUC and scaffold+LUC samples in the experiment without PEI and the staples+LUC sample showed the greatest activity. This suggest that the components of the origami assist in transfection. However, the LUC-origami seems to enter cells better than the LUC+staples and LUC+scaffold when PEI is included. Two right-side histograms show the luminescence intensity for the filtered LUC-origami (LUC-HTB), free LUC and bare origami (HTB). The results suggest that the origami entered cells better than the free LUC, as the filtered HTB+LUC sample possessed roughly 3 times as

high intensity as the free LUC. Both samples contained the same amount of LUC, since the concentration of the free LUC was titrated to match the decay kinetics of LUC+HTB before transfection. In addition, it seems that the samples were able to enter cells without a transfection reagent.

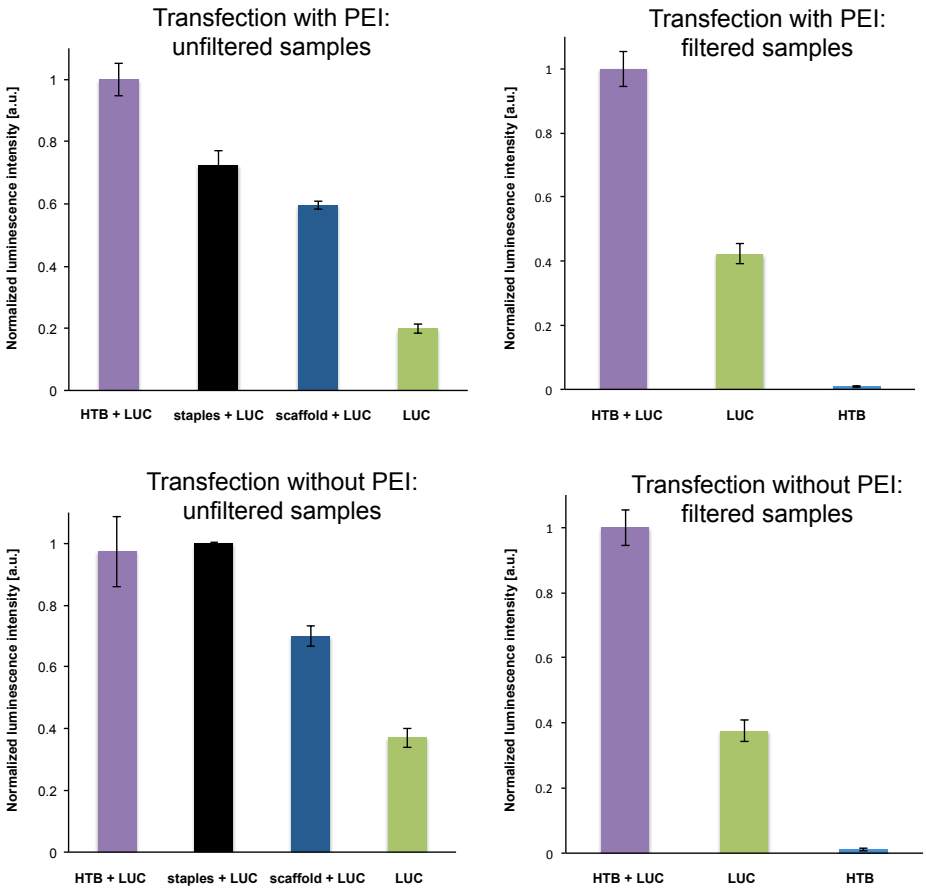

Figure 25: Normalized maximum luminescence intensities for the unfiltered LUC-HTB, staples+LUC, scaffold+LUC and free LUC, and for the spin-filtered HTB+LUC, free LUC and bare HTB with or without PEI. The bioluminescence intensities were measured from cell lysates after 12 h of transfection. The highest value in each measurement is normalized to 1. [104]

The effect of the nonspecific binding between LUC and HTB was studied further by fabricating a DNA origami that did not contain biotinylated binding sites (HT) for comparison. The HT sample was treated similarly as the HTB sample, and the same amount of luciferase enzyme was added to both of the samples. Spin-filtered LUC+HTB and LUC+HT were transfected to the cells (500 pM concentrations) and the bioluminescence assay was performed after 48 h of transfection from the cell lysates similarly as described earlier. The results are not directly comparable to other transfection results, since the samples were incubated for 48 h and not for 12 h.

Figure 26 shows the normalized maximum luminescence intensity for the LUC-HTB and LUC-HT samples. The LUC-HTB sample showed greater activity than the LUC-HT sample. The activity of HT sample was about 20 % of LUC+HTB signal, indicating that LUC can bind unspecifically to the origami surface. However, when the bioluminescence was measured from the HEPES-NaOH buffer before transfection experiments, the enzyme activity was the same for LUC+HTB and LUC+HT samples. One explanation for this might be that the methods used in transfection experiments might have removed the majority of nonspecifically bound LUC-enzymes but not the LUC-enzymes that are bound via strong biotin-streptavidin interaction. Overall, the used method could be considered rather feasible, since the lowest DNA origami working concentrations were approximately 500 pM - 1 nM.

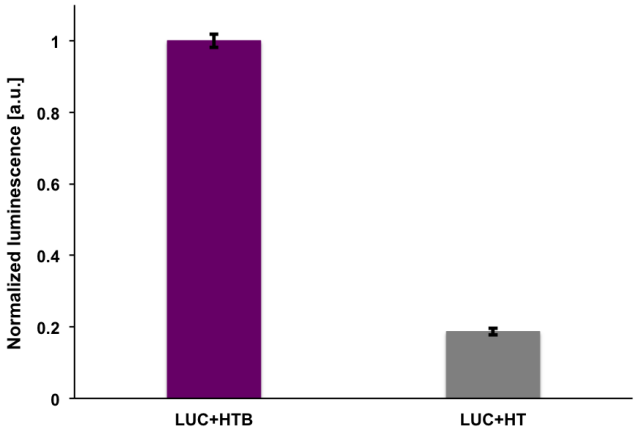

Figure 26: Normalized maximum luminescence intensity for the LUC-origami with biotinylated binding sites (LUC-HTB) and without biotinylated binding sites (LUC-HT) measured from the cell lysates after 48 h of transfection.

7 Conclusions

The aim of this thesis was to utilize a tubular DNA origami nanocarrier to deliver enzymes into cells. The delivered enzyme was streptavidin functionalized Lucia luciferase (LUC) that was detected by a bioluminescence assay and the transfection was also studied by a confocal microscopy. The results suggest that the DNA origami could be used for delivering enzymes into cells, and that the enzymes can remain active after transfection. Moreover, it seems that a tubular DNA origami can be transfected into cells without the transfection reagent. However, the components of the origami seemed to assist in transfection, and therefore the shape of the origami might not have contributed to the transfection. In addition, the integrity and stability of the DNA origamis should be studied further to prove the successful use of these DNA origamis as delivery vehicles. The structure of nanotubes should be characterized by TEM after adding the LUC-enzymes and the transfection reagent PEI to verify that the DNA origamis are stayed intact. The cytotoxicity of PEI to cell viability should be examined for PEI-mediated uptake experiments. Moreover, the cell uptake experiments for confocal microscopy were run over 36 h which is quite a long incubation time. The confocal images should be taken after 12 h and the possible degradation of the DNA origamis in cell culture media must be investigated carefully. Furthermore, the enzymes could be labeled fluorescently in order to investigate the co-localization of the enzymes and the origamis in cells. These examinations were not done in this thesis due to limited schedule.

Another target of this thesis was to examine the enzyme activity of polymer coated DNA origamis loaded with LUC-enzymes. The findings suggest that by adjusting the amount of cationic polymers that coat the DNA origamis, it could be possible to control the enzyme kinetics of the complexes. The thickest polymer coatings seemed to prolong the reaction rates of the enzyme reactions. In future experiments the cytotoxicity of the complexes should be studied to verify their suitability for cellular environments. Such a polymer coated origami system could also be possibly utilized to protect the molecular cargo attached to origamis.

One obstacle in this thesis arose from the fact that the proposed origami was not able to spatially organize the enzymes. The DNA origamis contained three biotinylated binding sites for the attachment of the LUC-enzymes, however it was noticed that the enzymes most likely attached to the origamis nonspecifically. Therefore, it was difficult to determine the real enzyme concentration of the samples. In order to utilize the same amount of enzymes in the control samples (free LUC-enzymes), the concentration of the free LUC samples was titrated to match the decay kinetics of LUC-origami samples. Additional experiments should be performed to limit the nonspecific binding. One approach is to reduce the ionic interaction between the enzyme and the origami by modifying the salt concentration. Another approach is to vary the pH to change the charge of the enzyme.

The successful cellular delivery of enzymes is important in various therapeutic applications. Recent study [5] showed that enzymes coated by DNA strands can be delivered into cells and retain their activity in cells. DNA origami nanocarriers could enable further specified cell targeting due to the possibility of modifications and the

modularity of DNA origamis. Moreover, it has been shown that the encapsulation of enzymes using DNA origami could protect them against protease digestion [109]. However, the proposed origami carrier in this thesis cannot accomplish these properties because of the nonspecific binding of the enzymes. If the problems related to nonspecific binding can be resolved, future works could include encapsulation of the origami system by virus capsid proteins, which has shown to improve the delivery of origamis into cells [34]. In addition, it would be interesting to examine the effect of the polymer coatings on the transfection rates of DNA origamis.

References

[1] N. C. Seeman, "Nucleic acid junctions and lattices," *Journal of Theoretical Biology*, vol. 99, no. 2, pp. 237–247, 1982.

[2] V. Linko and H. Dietz, "The enabled state of DNA nanotechnology," *Current Opinion in Biotechnology*, vol. 24, no. 4, pp. 555–561, 2013.

[3] J. Li, C. Fan, H. Pei, J. Shi, and Q. Huang, "Smart drug delivery nanocarriers with self-assembled DNA nanostructures," *Advanced Materials*, vol. 25, no. 32, pp. 4386–4396, 2013.

[4] V. Linko, A. Ora, and M. A. Kostiainen, "DNA nanostructures as smart drug-delivery vehicles and molecular devices," *Trends in Biotechnology*, vol. 33, no. 10, pp. 586–594, 2015.

[5] J. D. Brodin, A. J. Sprangers, J. R. McMillan, and C. A. Mirkin, "DNA-mediated cellular delivery of functional enzymes," *Journal of the American Chemical Society*, vol. 137, no. 47, pp. 14838–14841, 2015.

[6] D. Yang, M. J. Campolongo, T. N. Nhi Tran, R. C. H. Ruiz, J. S. Kahn, and D. Luo, "Novel DNA materials and their applications," *Wiley Interdisciplinary Reviews: Nanomedicine and Nanobiotechnology*, vol. 2, no. 6, pp. 648–669, 2010.

[7] C. Lin, Y. Liu, and H. Yan, "Designer DNA nanoarchitectures," *Biochemistry*, vol. 48, no. 8, pp. 1663–1674, 2009.

[8] L. Stryer, "Biochemistry," W. H. Freeman and Company, 4th ed., pp. 74–83, 2000.

[9] D. L. Nelson and M. M. Cox, "Lehninger Principles of Biochemistry," W. H. Freeman, 4th ed., pp. 11, 273, 2004.

[10] J. Kuriyan, B. Konforti, and D. Wemmer, "The molecules of life," p. 897, ISBN 978-0-8153-4188-8, 2013.

[11] V. Linko, "DNA-based applications in molecular electronics," PhD thesis, University of Jyväskylä, Department of Physics, Jyväskylä, pp. 120, 2011.

[12] G. M. Blackburn, M. J. Gait, D. Loakes, and D. M. Williams, "Nucleic acids in chemistry and biology," Cambridge, Royal Society of Chemistry, 3rd ed., pp. 13–72, 2006.

[13] N. C. Seeman, "An overview of structural DNA nanotechnology," *Molecular Biotechnology*, vol. 37, no. 3, pp. 246–257, 2007.

[14] L. A. Yatsunyk, O. Mendoza, and J.-L. Mergny, "Nano-oddities: Unusual nucleic acid assemblies for DNA-based nanostructures and nanodevices," *Accounts of Chemical Research*, vol. 47, no. 6, pp. 1836–1844, 2014.

[15] N. C. Seeman, "Nanomaterials based on DNA," *Annual Review of Biochemistry*, vol. 79, no. 1, pp. 65–87, 2010.

[16] F. Zhang, J. Nangreave, Y. Liu, and H. Yan, "Structural DNA nanotechnology: State of the art and future perspective," *Journal of the American Chemical Society*, vol. 136, no. 32, pp. 11198–11211, 2014.

[17] N. C. Seeman, "DNA in a material world," *Nature*, vol. 421, no. 6921, p. 427, 2003.

[18] S. H. Park, P. Yin, Y. Liu, J. H. Reif, T. H. LaBean, and H. Yan, "Programmable DNA self-assemblies for nanoscale organization of ligands and proteins," *Nano Letters*, vol. 5, no. 4, pp. 729–733, 2005.

[19] J. Zheng, P. E. Constantinou, C. Micheel, A. P. Alivisatos, R. A. Kiehl, and N. C. Seeman, "Two-dimensional nanoparticle arrays show the organizational power of robust DNA motifs," *Nano Letters*, vol. 6, no. 7, pp. 1502–1504, 2006.

[20] D. Smith, V. Schüller, C. Engst, J. Rädler, and T. Liedl, "Nucleic acid nanostructures for biomedical applications," *Nanomedicine*, vol. 8, no. 1, pp. 105–121, 2013.

[21] J. Li, H. Pei, B. Zhu, L. Liang, M. Wei, Y. He, N. Chen, D. Li, Q. Huang, and C. Fan, "Self-assembled multivalent DNA nanostructures for noninvasive intracellular delivery of immunostimulatory CpG oligonucleotides," *ACS Nano*, vol. 5, no. 11, pp. 8783–8789, 2011.

[22] Q. Jiang, C. Song, J. Nangreave, X. Liu, L. Lin, D. Qiu, Z.-G. Wang, G. Zou, X. Liang, H. Yan, and B. Ding, "DNA origami as a carrier for circumvention of drug resistance," *Journal of the American Chemical Society*, vol. 134, no. 32, pp. 13396–13403, 2012.

[23] V. J. Schüller, S. Heidegger, N. Sandholzer, P. C. Nickels, N. A. Suhartha, S. Endres, C. Bourquin, and T. Liedl, "Cellular immunostimulation by CpG-sequence-coated DNA origami structures," *ACS Nano*, vol. 5, no. 12, pp. 9696–9702, 2011.

[24] Q. Zhang, Q. Jiang, N. Li, L. Dai, Q. Liu, L. Song, J. Wang, Y. Li, J. Tian, B. Ding, and Y. Du, "DNA origami as an in vivo drug delivery vehicle for cancer therapy," *ACS Nano*, vol. 8, no. 7, pp. 6633–6643, 2014.

[25] H. Lee, A. Lytton-Jean, Y. Chen, K. Love, A. Park, E. Karagiannis, A. Sehgal, W. Querbes, C. Zurenko, M. Jayaraman, C. Peng, K. Charisse, A. Borodovsky, M. Manoharan, J. Donahoe, J. Truelove, M. Nahrendorf, R. Langer, and D. Anderson, "Molecularly self-assembled nucleic acid nanoparticles for targeted in vivo siRNA delivery," *Nature Nanotechnology*, vol. 7, no. 6, pp. 389–393, 2012.

[26] J.-W. Keum and H. Bermudez, "Enhanced resistance of DNA nanostructures to enzymatic digestion," *Chemical Communications*, pp. 7036–7038, 2009.

[27] C. Castro, F. Kilchherr, D.-N. Kim, E. Shiao, T. Wauer, P. Wortmann, M. Bathe, and H. Dietz, "A primer to scaffolded DNA origami," *Nature Methods*, vol. 8, no. 3, pp. 221–229, 2011.

[28] Q. Mei, X. Wei, F. Su, Y. Liu, C. Youngbull, R. Johnson, S. Lindsay, H. Yan, and D. Meldrum, "Stability of DNA origami nanoarrays in cell lysate," *Nano Letters*, vol. 11, no. 4, pp. 1477–1482, 2011.

[29] J. Hahn, S. F. J. Wickham, W. M. Shih, and S. D. Perrault, "Addressing the instability of DNA nanostructures in tissue culture," *ACS Nano*, vol. 8, no. 9, pp. 8765–8775, 2014.

[30] E. Benson, A. Mohammed, J. Gardell, S. Masich, E. Czeizler, P. Orponen, and B. Högberg, "DNA rendering of polyhedral meshes at the nanoscale," *Nature*, vol. 523, no. 7561, pp. 441–444, 2015.

[31] A. Walsh, H. Yin, C. Erben, M. Wood, and A. Turberfield, "DNA cage delivery to mammalian cells," *ACS Nano*, vol. 5, no. 7, pp. 5427–5432, 2011.

[32] J. W. Conway, C. K. McLaughlin, K. J. Castor, and H. Sleiman, "DNA nanostructure serum stability: greater than the sum of its parts," *Chemical Communications*, vol. 49, pp. 1172–1174, 2013.

[33] S. Perrault and W. Shih, "Virus-inspired membrane encapsulation of DNA nanostructures to achieve in vivo stability," *ACS Nano*, vol. 8, no. 5, pp. 5132–5140, 2014.

[34] J. Mikkilä, A.-P. Eskelinen, E. H. Niemelä, V. Linko, M. J. Frilander, P. Törmä, and M. A. Kostiainen, "Virus-encapsulated DNA origami nanostructures for cellular delivery," *Nano Letters*, vol. 14, no. 4, pp. 2196–2200, 2014.

[35] P. W. K. Rothemund, "Folding DNA to create nanoscale shapes and patterns," *Nature*, vol. 440, no. 7082, pp. 297–302, 2006.

[36] B. Saccà and C. M. Niemeyer, "DNA origami: The art of folding DNA," *Angewandte Chemie International Edition*, vol. 51, no. 1, pp. 58–66, 2012.

[37] J. Nangreave, D. Han, Y. Liu, and H. Yan, "DNA origami: a history and current perspective," *Current Opinion in Chemical Biology*, vol. 14, no. 5, pp. 608 – 615, 2010.

[38] D. Han, S. Pal, J. Nangreave, Z. Deng, Y. Liu, and H. Yan, "DNA origami with complex curvatures in three-dimensional space," *Science*, vol. 332, no. 6027, pp. 342–346, 2011.

[39] H. Said, V. J. Schüller, F. J. Eber, C. Wege, T. Liedl, and C. Richert, "M1.3–a small scaffold for DNA origami," *Nanoscale*, vol. 5, no. 1, pp. 284–290, 2013.

[40] B. Högberg, T. Liedl, and W. M. Shih, "Folding DNA origami from a double-stranded source of scaffold," *Journal of the American Chemical Society*, vol. 131, no. 26, pp. 9154–9155, 2009.

[41] S. Douglas, A. Marblestone, S. Teerapittayanon, A. Vazquez, G. Church, and W. Shih, "Rapid prototyping of 3D DNA-origami shapes with caDNAno," *Nucleic Acids Research*, vol. 37, no. 15, pp. 5001–5006, 2009.

[42] J.-P. J. Sobczak, T. G. Martin, T. Gerling, and H. Dietz, "Rapid folding of DNA into nanoscale shapes at constant temperature," *Science*, vol. 338, no. 6113, pp. 1458–1461, 2012.

[43] A. Shaw, E. Benson, and B. Högberg, "Purification of functionalized DNA origami nanostructures," *ACS Nano*, vol. 9, no. 5, pp. 4968–4975, 2015.

[44] T. Tørring, N. V. Voigt, J. Nangreave, H. Yan, and K. V. Gothelf, "DNA origami: a quantum leap for self-assembly of complex structures," *Chemical Society Reviews*, vol. 40, pp. 5636–5646, 2011.

[45] Z. Zhao, H. Yan, and Y. Liu, "A route to scale up DNA origami using DNA tiles as folding staples," *Angewandte Chemie International Edition*, vol. 49, no. 8, pp. 1414–1417, 2010.

[46] Z. Zhao, Y. Liu, and H. Yan, "Organizing DNA origami tiles into larger structures using preformed scaffold frames," *Nano Letters*, vol. 11, no. 7, pp. 2997–3002, 2011.

[47] Y. Yang, D. Han, J. Nangreave, Y. Liu, and H. Yan, "DNA origami with double-stranded DNA as a unified scaffold," *ACS Nano*, vol. 6, no. 9, pp. 8209–8215, 2012.

[48] A. Rajendran, M. Endo, Y. Katsuda, K. Hidaka, and H. Sugiyama, "Programmed two-dimensional self-assembly of multiple DNA origami jigsaw pieces," *ACS Nano*, vol. 5, no. 1, pp. 665–671, 2011.

[49] S. M. Douglas, H. Dietz, T. Liedl, B. Högberg, F. Graf, and W. M. Shih, "Self-assembly of DNA into nanoscale three-dimensional shapes," *Nature*, vol. 459, no. 7245, pp. 414–418, 2009.

[50] E. S. Andersen, M. Dong, M. M. Nielsen, K. Jahn, R. Subramani, W. Mamdouh, M. M. Golas, B. Sander, H. Stark, C. L. P. Oliveira, J. S. Pedersen, V. Birkedal, F. Besenbacher, K. V. Gothelf, and J. Kjems, "Self-assembly of a nanoscale DNA box with a controllable lid," *Nature*, vol. 459, no. 7243, pp. 73–76, 2009.

[51] H. Dietz, S. M. Douglas, and W. M. Shih, "Folding DNA into twisted and curved nanoscale shapes," *Science*, vol. 325, no. 5941, pp. 725–730, 2009.

[52] D. Han, S. Pal, Y. Liu, and H. Yan, "Folding and cutting DNA into reconfigurable topological nanostructures," *Nature Nanotechnology*, vol. 5, no. 10, pp. 712–717, 2010.

[53] T. Liedl, B. Högberg, J. Tytell, D. E. Ingber, and W. M. Shih, "Self-assembly of three-dimensional prestressed tensegrity structures from DNA," *Nature Nanotechnology*, vol. 5, no. 7, pp. 520–524, 2010.

[54] Y. Ke, L. L. Ong, W. M. Shih, and P. Yin, "Three-dimensional structures self-assembled from DNA bricks," *Science*, vol. 338, no. 6111, pp. 1177–1183, 2012.

[55] D. Han, S. Pal, Y. Yang, S. Jiang, J. Nangreave, Y. Liu, and H. Yan, "DNA gridiron nanostructures based on four-arm junctions," *Science*, vol. 339, no. 6126, pp. 1412–1415, 2013.

[56] A. Kuzuya and M. Komiyama, "DNA origami: fold, stick, and beyond," *Nanoscale*, vol. 2, no. 3, pp. 310–322, 2010.

[57] A. Kuzyk, K. T. Laitinen, and P. Törmä, "DNA origami as a nanoscale template for protein assembly," *Nanotechnology*, vol. 20, no. 23, p. 235305, 2009.

[58] A. Rajendran, M. Endo, and H. Sugiyama, "Single-molecule analysis using DNA origami," *Angewandte Chemie*, vol. 51, no. 4, pp. 874–890, 2012.

[59] Y. Ke, S. Lindsay, Y. Chang, Y. Liu, and H. Yan, "Self-assembled water-soluble nucleic acid probe tiles for label-free RNA hybridization assays," *Science*, vol. 319, no. 5860, pp. 180–183, 2008.

[60] H. K. K. Subramanian, B. Chakraborty, R. Sha, and N. C. Seeman, "The label-free unambiguous detection and symbolic display of single nucleotide polymorphisms on DNA origami," *Nano Letters*, vol. 11, no. 2, pp. 910–913, 2011.

[61] Y. Sannohe, M. Endo, Y. Katsuda, K. Hidaka, and H. Sugiyama, "Visualization of dynamic conformational switching of the g-quadruplex in a DNA nanostructure," *Journal of the American Chemical Society*, vol. 132, no. 46, pp. 16311–16313, 2010.

[62] S. Rinker, Y. Ke, Y. Liu, R. Chhabra, and H. Yan, "Self-assembled DNA nanostructures for distance-dependent multivalent ligand-protein binding," *Nature Nanotechnology*, vol. 3, no. 7, pp. 418–422, 2008.

[63] F. C. Simmel, "DNA-based assembly lines and nanofactories," *Current Opinion in Biotechnology*, vol. 23, no. 4, pp. 516–521, 2012.

[64] H. Gu, J. Chao, S.-J. Xiao, and N. C. Seeman, "A proximity-based programmable DNA nanoscale assembly line," *Nature*, vol. 465, no. 7295, pp. 202–205, 2010.

[65] N. D. Derr, B. S. Goodman, R. Jungmann, A. E. Leschziner, W. M. Shih, and S. L. Reck-Peterson, "Tug-of-war in motor protein ensembles revealed with a programmable DNA origami scaffold," *Science*, vol. 338, no. 6107, pp. 662–665, 2012.

[66] J. Liu, Y. Geng, E. Pound, S. Gyawali, J. R. Ashton, J. Hickey, A. T. Woolley, and J. N. Harb, "Metallization of branched DNA origami for nanoelectronic circuit fabrication," *ACS Nano*, vol. 5, no. 3, pp. 2240–2247, 2011.

[67] A. M. Hung, C. M. Micheel, L. D. Bozano, L. W. Osterbur, G. M. Wallraff, and J. N. Cha, "Large-area spatially ordered arrays of gold nanoparticles directed by lithographically confined DNA origami," *Nature Nanotechnology*, vol. 5, no. 2, pp. 121–126, 2010.

[68] B. Shen, V. Linko, H. Dietz, and J. J. Toppari, "Dielectrophoretic trapping of multilayer DNA origami nanostructures and DNA origami-induced local destruction of silicon dioxide," *Electrophoresis*, vol. 36, no. 2, pp. 255–262, 2015.

[69] H. T. Maune, S.-P. Han, R. D. Barish, M. Bockrath, W. A. Goddard III, P. W. K. Rothemund, and E. Winfree, "Self-assembly of carbon nanotubes into two-dimensional geometries using DNA origami templates," *Nature Nanotechnology*, vol. 5, no. 1, pp. 61–66, 2010.

[70] A. Kuzyk, R. Schreiber, Z. Fan, G. Pardatscher, E.-M. Roller, A. Högele, F. C. Simmel, A. O. Govorov, and T. Liedl, "DNA-based self-assembly of chiral plasmonic nanostructures with tailored optical response," *Nature*, vol. 483, no. 7389, pp. 311–314, 2012.

[71] C. Steinhauer, R. Jungmann, T. L. Sobey, F. C. Simmel, and P. Tinnefeld, "DNA origami as a nanoscopic ruler for super-resolution microscopy," *Angewandte Chemie*, vol. 48, no. 47, pp. 8870–8873, 2009.

[72] C. Lin, R. Jungmann, A. M. Leifer, C. Li, D. Levner, G. M. Church, W. M. Shih, and P. Yin, "Submicrometre geometrically encoded fluorescent barcodes self-assembled from DNA," *Nature Chemistry*, vol. 4, no. 10, pp. 832–839, 2012.

[73] M. J. Berardi, W. M. Shih, S. C. Harrison, and J. J. Chou, "Mitochondrial uncoupling protein 2 structure determined by NMR molecular fragment searching," *Nature*, vol. 476, no. 7358, pp. 109–113, 2011.

[74] R. Núñez-Lozano, M. Cano, B. Pimentel, and G. de la Cueva-Méndez, "'Smartening' anticancer therapeutic nanosystems using biomolecules," *Current Opinion in Biotechnology*, vol. 35, pp. 135–140, 2015.

[75] C. Wu, D. Han, T. Chen, L. Peng, G. Zhu, M. You, L. Qiu, K. Sefah, X. Zhang, and W. Tan, "Building a multifunctional aptamer-based DNA nanoassembly for targeted cancer therapy," *Journal of the American Chemical Society*, vol. 135, no. 49, pp. 18644–18650, 2013.

[76] O. C. Farokhzad and R. Langer, "Impact of nanotechnology on drug delivery," *ACS Nano*, vol. 3, no. 1, pp. 16–20, 2009.

[77] H. Hillaireau and P. Couvreur, "'Nanocarriers' entry into the cell: relevance to drug delivery," *Cellular and Molecular Life Sciences*, vol. 66, no. 17, pp. 2873–2896, 2009.

[78] P. Charoenphol and H. Bermudez, "Aptamer-targeted DNA nanostructures for therapeutic delivery," *Molecular Pharmaceutics*, vol. 11, no. 5, pp. 1721–1725, 2014.

[79] A. H. Okholm, J. S. Nielsen, M. Vinther, R. S. Sørensen, D. Schaffert, and J. Kjems, "Quantification of cellular uptake of DNA nanostructures by qPCR," *Methods*, vol. 67, no. 2, pp. 193–197, 2014.

[80] S. Ko, H. Liu, Y. Chen, and C. Mao, "DNA nanotubes as combinatorial vehicles for cellular delivery," *Biomacromolecules*, vol. 9, no. 11, pp. 3039–3043, 2008.

[81] J. Brglez, P. Nikolov, A. Angelin, and C. Niemeyer, "Designed intercalators for modification of DNA origami surface properties," *Chemistry - A European Journal*, vol. 21, no. 26, pp. 9440–9446, 2015.

[82] S. M. Douglas, I. Bachelet, and G. M. Church, "A logic-gated nanorobot for targeted transport of molecular payloads," *Science*, vol. 335, no. 6070, pp. 831–834, 2012.

[83] Y. Cho, J. B. Lee, and J. Hong, "Controlled release of an anti-cancer drug from DNA structured nano-films," *Scientific Reports*, vol. 4, p. 4078, 2014.

[84] C. Zhou, Z. Yang, and D. Liu, "Reversible regulation of protein binding affinity by a DNA machine," *Journal of the American Chemical Society*, vol. 134, no. 3, pp. 1416–1418, 2012.

[85] Y. Ke, J. Sharma, M. Liu, K. Jahn, Y. Liu, and H. Yan, "Scaffolded DNA origami of a DNA tetrahedron molecular container," *Nano Letters*, vol. 9, no. 6, pp. 2445–2447, 2009.

[86] A. Kuzuya and M. Komiyama, "Design and construction of a box-shaped 3D-DNA origami," *Chemical Communications*, pp. 4182–4184, 2009.

[87] Y.-X. Zhao, A. Shaw, X. Zeng, E. Benson, A. M. Nyström, and B. Högberg, "DNA origami delivery system for cancer therapy with tunable release properties," *ACS Nano*, vol. 6, no. 10, pp. 8684–8691, 2012.

[88] S. Kocabey, H. Meinl, I. S. MacPherson, V. Cassinelli, A. Manetto, S. Rothenfusser, T. Liedl, and F. S. Lichtenegger, "Cellular uptake of tile-assembled DNA nanotubes," *Nanomaterials*, vol. 5, pp. 47–60, 2015.

[89] K. Mohri, M. Nishikawa, N. Takahashi, T. Shiomi, N. Matsuoka, K. Ogawa, M. Endo, K. Hidaka, H. Sugiyama, Y. Takahashi, and Y. Takakura, "Design and development of nanosized DNA assemblies in polypod-like structures as efficient vehicles for immunostimulatory CpG motifs to immune cells," *ACS Nano*, vol. 6, no. 7, pp. 5931–5940, 2012.

[90] S. Sellner, S. Kocabey, K. Nekolla, F. Krombach, T. Liedl, and M. Rehberg, "DNA nanotubes as intracellular delivery vehicles in vivo," *Biomaterials*, vol. 53, pp. 453–463, 2015.

[91] X. Liu, Y. Xu, T. Yu, C. Clifford, Y. Liu, H. Yan, and Y. Chang, "A DNA nanostructure platform for directed assembly of synthetic vaccines," *Nano Letters*, vol. 12, no. 8, pp. 4254–4259, 2012.

[92] M. Liu, J. Fu, C. Hejesen, Y. Yang, N. W. Woodbury, K. Gothelf, Y. Liu, and H. Yan, "A DNA tweezer-actuated enzyme nanoreactor," *Nature Communications*, vol. 4, p. 2127, 2013.

[93] V. Linko, M. Eerikäinen, and M. A. Kostiainen, "A modular DNA origami-based enzyme cascade nanoreactor," *Chemical Communications*, vol. 51, pp. 5351–5354, 2015.

[94] R. Desnick and E. Schuchman, "Enzyme replacement therapy for lysosomal diseases: Lessons from 20 years of experience and remaining challenges," *Annual Review of Genomics and Human Genetics*, vol. 13, pp. 307–335, 2012.

[95] S. Muro, "New biotechnological and nanomedicine strategies for treatment of lysosomal storage disorders," *Wiley Interdisciplinary Reviews: Nanomedicine and Nanobiotechnology*, vol. 2, no. 2, pp. 189–204, 2010.

[96] J. Zawilska, J. Wojcieszak, and A. Olejniczak, "Prodrugs: A challenge for the drug development," *Pharmacological Reports*, vol. 65, no. 1, pp. 1–14, 2013.

[97] A. Z. Wang, R. Langer, and O. C. Farokhzad, "Nanoparticle delivery of cancer drugs," *Annual Review of Medicine*, vol. 63, no. 1, pp. 185–198, 2012.

[98] W. Sun and Z. Gu, "Engineering DNA scaffolds for delivery of anticancer therapeutics," *Biomaterials Science*, vol. 3, pp. 1018–1024, 2015.

[99] Y.-J. Chen, B. Groves, R. A. Muscat, and G. Seelig, "DNA nanotechnology from the test tube to the cell," *Nature Nanotechnology*, vol. 10, no. 9, pp. 748–760, 2015.

[100] A. V. Pinheiro, D. Han, W. M. Shih, and H. Yan, "Challenges and opportunities for structural DNA nanotechnology," *Nature Nanotechnology*, vol. 6, no. 12, pp. 763–72, 2011.

[101] E. Stahl, T. G. Martin, F. Praetorius, and H. Dietz, "Facile and scalable preparation of pure and dense DNA origami solutions," *Angewandte Chemie International Edition*, vol. 53, no. 47, pp. 12735–12740, 2014.

[102] B. Kick, F. Praetorius, H. Dietz, and D. Weuster-Botz, "Efficient production of single-stranded phage DNA as scaffolds for DNA origami," *Nano Letters*, vol. 15, no. 7, pp. 4672–4676, 2015.

[103] E. Pound, J. R. Ashton, H. A. Becerril, and A. T. Woolley, "Polymerase chain reaction based scaffold preparation for the production of thin, branched DNA origami nanostructures of arbitrary sizes," *Nano Letters*, vol. 9, no. 12, pp. 4302–4305, 2009.

[104] A. Ora, E. Järvihaavisto, M. A. Kostiainen, and V. Linko, "Cellular delivery of enzyme-loaded DNA origami," manuscript in preparation, 2016.

[105] M. Eerikäinen, "DNA origami-based enzyme nanoreactor," Master's thesis, School of Electrical Engineering, Aalto University, Espoo, 2014.

[106] V. Linko, B. Shen, K. Tapio, J. J. Toppari, M. A. Kostiainen, and S. Tuukkanen, "One-step large-scale deposition of salt-free DNA origami nanostructures," *Scientific Reports*, vol. 5, p. 15634, 2015.

[107] J. K. Kiviaho, V. Linko, A. Ora, T. Tiainen, E. Järvihaavisto, J. Mikkilä, H. Tenhu, Nonappa, and M. A. Kostiainen, "Cationic polymers for DNA origami coating – examining the binding efficiency and tuning the enzymatic reaction rates," *Nanoscale*, under review, 2016.

[108] M. Berberan-Santos, E. Bodunov, and B. Valeur, "Mathematical functions for the analysis of luminescence decays with underlying distributions 1. Kohlrausch decay function (stretched exponential)," *Chemical Physics*, vol. 315, no. 1–2, pp. 171–182, 2005.

[109] Z. Zhao, J. Fu, S. Dhakal, A. Johnson-Buck, M. Liu, T. Zhang, N. Woodbury, Y. Liu, N. Walter, and H. Yan, "Nanocaged enzymes with enhanced catalytic activity and increased stability against protease digestion," *Nature Communications*, vol. 7, 2016.

A Strands for DNA origami

The complete set of the staple strands for DNA origami are listed below. More information is available from the Ref. [93].

Biotinylated strands for HTB (3 strands):

Sequence (5' -> 3')	**Bases**
Biotin-AAACATTAAATTTTGCTCCAACACGTTG	28
Biotin-AGCTTTCAACATTAAATAGTGAATTTGCCAGAATGATTGAC	41
Biotin-ACGAGGCAATTCCAACGAAACGCAAAGACGTTCAGCTA	38

Non-biotinylated strands for HT, optional, replaces the above-mentioned strands (3 strands):

Sequence (5' -> 3')	**Bases**
AAACATTAAATTTTGCTCCAACACGTTG	28
AGCTTTCAACATTAAATAGTGAATTTGCCAGAATGATTGAC	41
ACGAGGCAATTCCAACGAAACGCAAAGACGTTCAGCTA	38

Cy3-labeled fluorescent strand, optional (1 strand):

Sequence (5' -> 3')	**Bases**
Cy3-GGGAAAGGAGAAAAAA	16

Binding sites for the Cy3-labeled strand (5 strands):

Sequence (5' -> 3')	**Bases**
CAACTAATCATAACCAGACGACTGGATAGCGTTTTTTTCT-CCTTTCCC	48
TGGTCAGTACAGTTGACAGGTCAGTTTTTTCTCCTTTCCC	40
CCAAGCGGCCTGATGAAATCCTGAAAGAGGACATTTTTT-CTCCTTTCCC	49
GAATACGAAACCGGATAGCCAAGCCCTTTTTAAGAATTTT-TTCTCCTTTCCC	52
AAGCTTGAATCATGGTTTTTTTCTCCTTTCCC	32

Core strands (91 strands):

Sequence (5' -> 3')	**Bases**
CGTAATACATCAACATCTGGCC	22
AGGCAATGCAGCTGATTGCCTTAAACGGGCCTAAAAA-GGCGTTGCTTATC	50
CAATCCAATTTATTTACTCATCCAACATATAAAAGAGCA-TGTAAAACCAA	50
TATATTTAGGATAAATGACCCAAGAATT	28
TTTCACCGCAGCAACCGCGAAAGAC	25

AATTCGGAAAAGCCCTATAGCCCGGAAAATATAATCAATTGATA	44
GAGCTGCTCAGAGAAAATACGTGAGGC	27
AATATGATACAAACTACAAGGTTTCAGGCCACCCTTCTAGGTGT	44
TAGTAAATTTCAACCCGAACCTCAA	25
AATTCACAGAGCCCTGACTATTATAATTATGTA	33
CGCGAGATCTTCTATAAGAACTGTTT	26
CAGCACCTTTTCATGGAAGGGCGCCAT	27
AATGCTTATAAATAAGTAAAATAACGGA	28
TTTCAGAAGATAAAACAGAGCGAACGAATATACGTGG	37
TCAATCACAGGTCAAGAACCGGATAGCA	28
TTGCCCTGACGATAATCATCTAAAGAA	27
CGATTAAGTTGGTGACCTTCAAAAGCTGGCGTTAAGACCTAA	42
ATCATTTTATCAGTTTGGATACGTAAATTTAACG	34
GAAATACGCATTTTCGAACCAGACAGCCAGGTTTGAGG	38
TGTTACTTGGGAACCTAGGCTGGCGTAACGCCAGGG	36
CTTGCTAAAAAAAAGTAGGATGGCTTAGA	29
CACAGACAATAGCCATTACATGGAA	25
TCACCCTCAGCAGAAATCGGCAACATTAGACG	32
TTGAAAACTCTGAGAAGGAGGTTGAAATCAAAATCATAGGATAGCGATAG	50
TTCCTGTAGTTACGAGGCATAAATAGCG	28
CGCCATTCGATCGGAAAGGGGACGTTGTGCAGGTCCGATTGACAAAGAC	49
GAAGCGTTGAGTTAAGCAATAGACGCTGGAGGGTGG	36
AGCCCAATCACCAGTATTCAAAAAGGGT	28
GGTCATTTTTGCGAACCCTCAGAGAAAGGCGGAGTGTCTTTCCAGACGT	49
ATCGGTTATAAAGCAAAAGGTTTAAAGGCCGCTGTTTAGCTATGGGGCGC	50
TGTGATGAAACCATAGCAAGCGCCATAGCATTTT	34
CTTAGATTGAGTGAATAATTTTCGTTGGGTCAATCG	36
GTACCGCTCATCGTAGGAATCCTATTATTTATCC	34
ATCACCGTACTCCACCCTCTTGCCTGGAGATCTACAAAGGCTGTCAGAAG	50
ACATGACATTCAACGACTCTAGAGGAAGACGGTCAATAAACA	42
AAGGTGGGAGAACACTTTCCAGAATCGG	28
GGCAGAGTTTAACAACGCCAAAGCACCAAGTCACGGATGTGCTGCAAGG	49
ACAGTCAAAGCGAAAAACAACTGAATTTTCTGTATGGGAAGG	42
TAATTGCTATAATGAAGTACGGTGTCTAAAGCTAAGCTTAATCATCAC	48

TACATTTGACGCCTGTAGCATTCCACAGTTTTGTC	35
AACGATTACCAGAAGCCAAAAGAACTGCAAGCCG-TTATAAGA	42
TATCGGTGAATTACCAAATCTAGGCTTAGCCTTAG-AATCC	40
TTCGCGTTAATGCCCCAGAGGAGAGGCTTTTGCA-AAACATTAAATTT	47
CACCCTAGCATTGACGACTACCTTTTTCACCCTCC-CGGAACGGTTT	46
TAAAGTGTAAACCTGTCGAAGAATACACTAACGCC-GGAAGCA	42
CGAAAAACCGTTGGAAATACAACTGAACACCCCGT-CAAAGGG	42
ACGCTCACTATCAAGCCATTGCTGACCT	28
TTTTTCTCCAACGCGTTTTTTGTTTAA	27
TTGAGTCACCCTCATATTTAGATTCAAATCACCATC	36
ATAACCGATACCACCAGCTTAAACAGCTTGCATCG-CCCACGC	42
TGAAACAAACATCTGAGTAACTATTTCGGAAGGATT-AGGATGCGTAG	47
AGTATCGTCACCAATAAATAAGCTCATTC	29
GGACGAACTAACGGAGGGATAGGTCACTCTGCCA-CTTTCCG	41
GGTCAGTTCTAAAGTGCTGAATCCTTTTGATAAGA	35
AGTTGAGGGAAGAATTATGCGTCAACTTGAAACAC-ACGTAAC	42
GAAAGCGTAAGAATTCGGTCGCAGGGAGGGCATCA	35
TCAGATGGAAACAATGTTTAGACGATAA	28
TAATTTTCAAACAAATATCGCGGAAGCA	28
CGAGCCAGACGACAATCATAAAGCCGGA	28
GGAGAATTCTACATTTTAACGAGCGTATAAAAACAGG	37
TTTTCCCTTACCATTCGATAG	21
ATTCTACAGCAAAATTAAGCAGTACCAA	28
CGGGCAACCAGCTGATAAACAGCCATAAGAACGCG-CGAAAG	41
CGGTATTATTACCGGGGTATTGAAACCATCCCATC	35
CAAGACCAGAGCCGCAACCTCCCGTTAATTAGAAA-GCGCCAAAAGGAACC	50
AGTGACAACTGTTGCGCGACCG	22
TCAAGAGAGGCGCAGAACTGAAATTCTGTATCAAC-AATAGA	41
GCCTGTTTCCAGACGTAATAAGCTTAAT	28
GTTTTGCTCAGATATAAGCAAAAACTAGCATG	32
ATTTTCAGGACAGAAATAAAGAAATTTAGCGGG	33
GCCTAAATCAAGATCACTTCACCGCCTGCGAGGGT-CTTTTGCGGGATCG	49

GGTGGTTGCGGTCCCTTTTACAGAGAGAATAACCT-TTCCAGA	42
AAAAGGGCACCACGTGTTATCGGGTGCC	28
ATTTGACAATATATGTAAGACGCTGAGACATTTAGC-AAAAGCACTGATTG	50
CTTTGAATACCATTTCAATCAACACTATGCAGATAC-ATAAATTCATC	47
GAGAATAATTTTTTAAGGAGCGAGGTGAA	29
CGTCAAAACATTAATGTCGGGAAAGCCTGCGCTC-ACGCTCCCCGGGTACC	50
ATATCAAACCTTTTGCTCCAGACCGTTTTAAGCAT-CAAATCAGGT	45
TTGAGGACTCAATCTGAAAAA	21
CCCCGGTCCCCCTCACTTTACCACAACATT	30
CAAAATTAATTAAGAGTCTTACAGGAAAACGACGACAG	38
CAAAGCGGATTTTCGAGCAGTATTATAGATAA	32
AGCATCGGAAGCCCTGAGAGAGTTAGTGAGA	31
TCAGGCTGCGCACTCGCCACCAAGAACCGC	30
ATCAGAAGTTTTGCCCTGCCAGTGCCCGTATAAAA-AGATGA	41
GGGTAATTTCATTGCTGATTGATGATGGC	29
GAGCTCGGTGAAATGAATAAGATACATA	28
AAACCAAGTAAGAGTACCTGAACAATTTC	29
ATGCAGAACGCCTAATTTCACAAC	24
ATTTAATCGCCTCCTGCCTCAGGAAGATCGATAAGGC	37
AAAATCTAGTTTCAGCCGGAG	21

Left core strands (20 strands):

Sequence (5' -> 3')	**Bases**
CTGCGGCTGAATACATCATA	20
ATTAACAAAACATCTTTTTGAAACCCTTCAACACGACCAGT	41
AAGAAATATCATCCGAAACA	20
TATTTGCTATACTTAATCGTCTAAACAGTTCAGAAAACGA	40
AAAAGCTAAACACCAAATCACAGAACGAGTAGTAAA	36
TGCGGGAGGTTTTGAAGCCTTAATTTGCCAGTTACAAAATG-AAAATA	47
ACTAACAACTAATAGATTAGAGCCGTCAAGACTTTAAAAAGT	42
GTTTCATCGTCATTTATTTAGAAATGGTTGAAATGG	36
CAAATCTATATAAGACGTTGATTTAGGAA	29
GACTTCAATTCGACAACT	18
ATCGGGAAATATACTCAAAAT	21
AAGTACAAAACACTCAAGAACCGCCCAATAGCAA	34
GAATGACCATAAACAAAGAACGTTAT	26
TACAATTTTATCCTGAATCTTACCAACGCTGACGCTC	37
ATACGAGGAGATTTGAATAATAATCAATAATCGGCTGT	38

TTCACCAGTCACAGGAAAAAATCGTCCAATAACAGCAACG	40
TGAGAATGCCGGAAACATATGCGTTATACAGTAGGGAGAA-TATAAAGT	48
ATTAATTAACCTTGCATAAATATTACCT	28
TAAAGTCCAACTTGCGACCTGCTCCA	26
CAACTACTGTAGCCAGCAAAAATATC	26

Right core strands (15 strands):

Sequence (5' -> 3')	**Bases**
TCGATGAACGGTAATCGTAAAACAGGAAGAAATATTTTT-ATTCT	44
TAATAGTGTTGAGTGTGCTTGCTGAGTGTTCCAGTTTG-GAACAAG	45
AGGTAAAGATTCACCGTTCTTTTTTGAAGAGTCTGGAG-CAAACAAGAGAA	50
CGTTCCAGTAAGCGTCATACATGGCAAGAAAA	32
TGAGCGAACGGCGGGAAAGCGATAAATC	28
TAATGAGCTGCCCGAGGCATGATTAAGAAAAATACTTT-ATTTTGT	45
AGTTTTAACGGGGTCAGTGCCTTTTTGATGATTCGCGT-TAAATG	44
CTCATTAAGGCAGGTCAGACGATT	24
GTCATAGTAGCGCGGTAATCACACCAGTCACCGTCAC-CGACTTGA	45
TAACCGTGCAGTTGGTGCCAGAGCCGCCGCCCAGAG-CCTCACCGG	45
TTACCAGCGCGGGAGGGGGTGAATTATCATGTAATTTA	38
CTGAGTTTCGTAGGAACGAACCGCAGGAGGTAGGGTTG	38
GCAGCCATCTTACCGGAACAAAGCGGGGAGAGGCGGT	37
AAGAACGTGGACTCCAATGAACAAAGTCAGAGGGTAAT-TGAGCGCTA	47
TACCAGGGAGACTCCTCAAGAGAACCTATGTTAA	34

B Luminescence assay for filtered and unfiltered Streptavidin-Lucia enzyme

Figure B1 shows that the spin-filtering procedure was efficient for removing free LUC-enzymes. The first data points are measured around 10 seconds after adding the substrate, and thus the measured maximum intensities do not directly compare to the actual LUC concentrations.

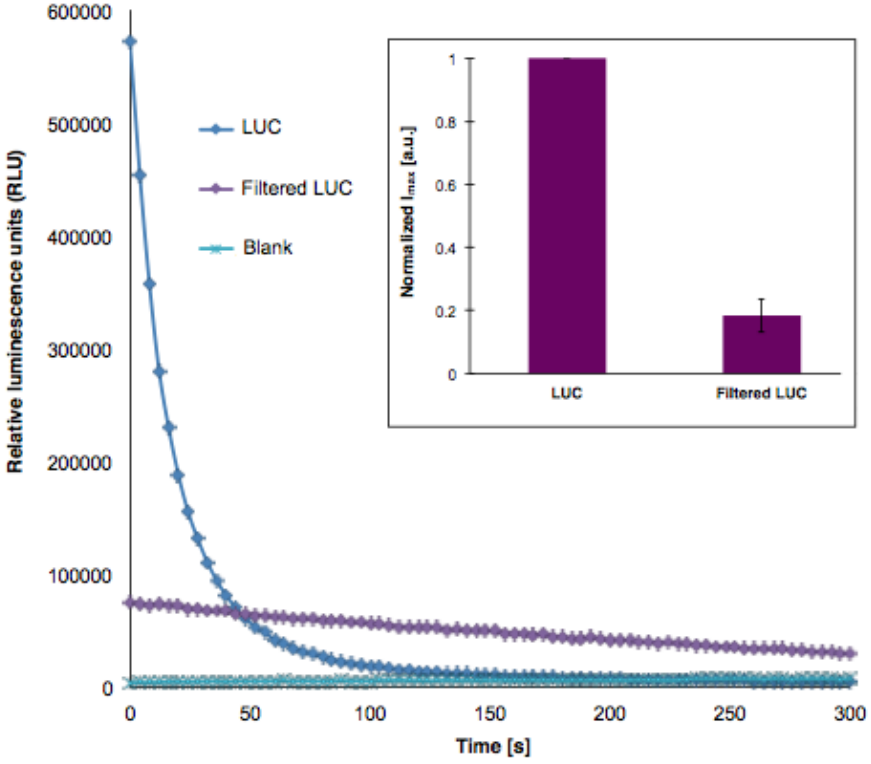

Figure B1: Luminescence decay and the normalized maximum luminescence intensity for the plain free Streptavidin-Lucia (LUC) and the spin-filtered Streptavidin-Lucia (Filtered LUC).